Aerodynamics of Heavy Vehicles

Haecheon Choi,[1,2] Jungil Lee,[2,3] and Hyungmin Park[1]

[1]School of Mechanical and Aerospace Engineering and [2]Institute of Advanced Machinery and Design, Seoul National University, Seoul 151-744, Korea; email: choi@snu.ac.kr, hminpark@snu.ac.kr

[3]Department of Mechanical Engineering, Ajou University, Suwon 443-749, Korea; email: jungillee@ajou.ac.kr

Annu. Rev. Fluid Mech. 2014. 46:441–68

First published online as a Review in Advance on October 2, 2013

The *Annual Review of Fluid Mechanics* is online at fluid.annualreviews.org

This article's doi: 10.1146/annurev-fluid-011212-140616

Keywords

heavy vehicle, wake flow, underbody flow, gap flow, ground effect, crosswind effect, drag reduction

Abstract

We present an overview of the aerodynamics of heavy vehicles, such as tractor-trailers, high-speed trains, and buses. We introduce three-dimensional flow structures around simplified model vehicles and heavy vehicles and discuss the flow-control devices used for drag reduction. Finally, we suggest important unsteady flow structures to investigate for the enhancement of aerodynamic performance and future directions for experimental and numerical approaches.

1. INTRODUCTION

The flow around a heavy vehicle, including a tractor-trailer, bus, and high-speed train (HST), is inherently three dimensional and exhibits complex characteristics, such as a turbulent boundary layer, separation and reattachment on the vehicle surface, massive separation at the rear trailing edge, shear-layer evolution, and a large wake behind the vehicle. Furthermore, the Reynolds number is so high that a turbulent boundary-layer flow develops above most of the vehicle's surface, except very near the front surface. Understanding the effects of these flow characteristics on the vehicle's aerodynamic performance has considerable practical significance because they are closely related to fuel economy, greenhouse gas emission, driving stability, etc. For example, the massive separation at the blunt trailing edge of a vehicle results in a significant pressure drop at the base, which is one of the main sources of aerodynamic drag. Numerous studies have been conducted in both academia and industry to understand and control the flows around heavy vehicles (Ahmed et al. 1985, Baker 2010a, Cooper 2003, Hucho 1998, Hucho & Sovran 1993, Raghunathan et al. 2002). Drag reduction, in particular, has been one of the major concerns of heavy vehicle studies because it is directly related to energy savings; for example, one can achieve approximately 4% fuel savings by a 20% aerodynamic drag reduction at an operating speed of 105 km h^{-1} for a tractor-trailer weighing 36 tons (Bradley 2000). [Fuel consumption for a heavy vehicle at this speed includes engine losses owing to thermal efficiency (60%), aerodynamic losses (21%), losses owing to rolling resistance (13%), and other losses (6%).] Furthermore, rapid increases in fuel prices and the depletion of petroleum resources have made it more urgent to solve this issue. During the past few decades, vigorous investigations have been conducted to develop new flow-control methods and to improve existing ones in terms of drag reduction; these have been accompanied by an improved understanding of heavy vehicle aerodynamics. The main strategy for drag reduction for heavy vehicles has been to alter or weaken the flow structures responsible for generating aerodynamic drag, such as the undesirable flow separation from the surface of the vehicle.

In Section 2, we discuss various flow structures around heavy vehicles. First, we consider two well-known, simplified, three-dimensional model vehicles: the Ahmed (Ahmed et al. 1984) and GM (Han et al. 1996) models, which represent fast-back and square-back vehicles, respectively. We then discuss flow phenomena specific to the tractor-trailer, bus, and HST. In Section 3, we introduce various devices for forebody, base, and underbody drag reduction. Most previous studies have investigated the aerodynamics of heavy vehicles relying on mean flow characteristics, but the unsteady flow phenomena are much more related to the mechanism of aerodynamic force generation and its control. In Section 4, therefore, we identify important flow structures to investigate further. We also suggest future directions for experimental and numerical approaches for studying the flows around heavy vehicles at high Reynolds numbers.

2. FLOW CHARACTERISTICS AROUND HEAVY VEHICLES

The flows around ground vehicles, including the various heavy vehicles covered in this review, share unsteady and three-dimensional features with those around other aerial or marine transportation vehicles. However, in contrast to the flow around a commercial airplane, ship, or submarine, a key phenomenon in the flow around a ground vehicle is massive flow separation, which significantly affects the aerodynamic forces and moments experienced by the vehicle (Ahmed et al. 1985). This phenomenon is more pronounced for heavy vehicles that have a boxy shape with many sharp edges for carrying as much cargo and as many passengers as possible within regulated external dimensions (Ahmed et al. 1985, Bearman 2009, Ortega & Salari 2004). In this section, we introduce flow structures around heavy vehicles, focusing on the separated flows originating

Figure 1

Simplified, three-dimensional model vehicles and their geometrical relevance to heavy vehicles: (*a*) the Ahmed model and (*b*) the GM model.

from various locations on the vehicle. First, we discuss flows around two well-known, simplified, three-dimensional model vehicles: the Ahmed (Ahmed et al. 1984) and GM (Han et al. 1996) models. Next, we look into the detailed flow phenomena specific to the tractor-trailer, bus, and HST in turn.

2.1. General Features of Flow Around a Simplified Three-Dimensional Model Vehicle

In this section, we discuss three-dimensional flow structures around simplified three-dimensional model vehicles and the ground effect acting on these vehicles.

2.1.1. Three-dimensional flow structures. The generic geometry of a simplified three-dimensional model vehicle provides a good reference for studying the aerodynamics of real vehicles. Although various simplified model vehicles have been investigated (Le Good & Garry 2004), here we discuss flows around two models: the Ahmed (Ahmed et al. 1984) and GM (Han et al. 1996) models, which represent fast-back and square-back vehicles, respectively (**Figure 1**). The Ahmed model, proposed by Ahmed et al. (1984), has a slanted rear surface, making it feasible for use in studying the effect of a variable rear shape. By contrast, the GM model, proposed by General Motors (Han et al. 1996), has a square-back rear shape with a blunt trailing edge. The common features of the Ahmed and GM models are that they have a rounded forebody to prevent flow separation there, and a middle body with a rectangular cross section. Thus, the flow after the forebody develops into a turbulent boundary layer until it meets the trailing edge of the model vehicle, where it separates. We note that the Reynolds numbers for the Ahmed and GM model vehicles are $Re_H = u_\infty H/\nu = 1.18 \times 10^6$ and 1.7×10^5, respectively, where u_∞ is the free-stream velocity, H is the vehicle height, and ν is the kinematic viscosity. These Reynolds numbers are still lower than those of heavy vehicles [i.e., a tractor-trailer, bus, and HST; $Re_H = O(10^6)$], but the flow characteristics in the wake of the model vehicles should not be very different from those of heavy vehicles.

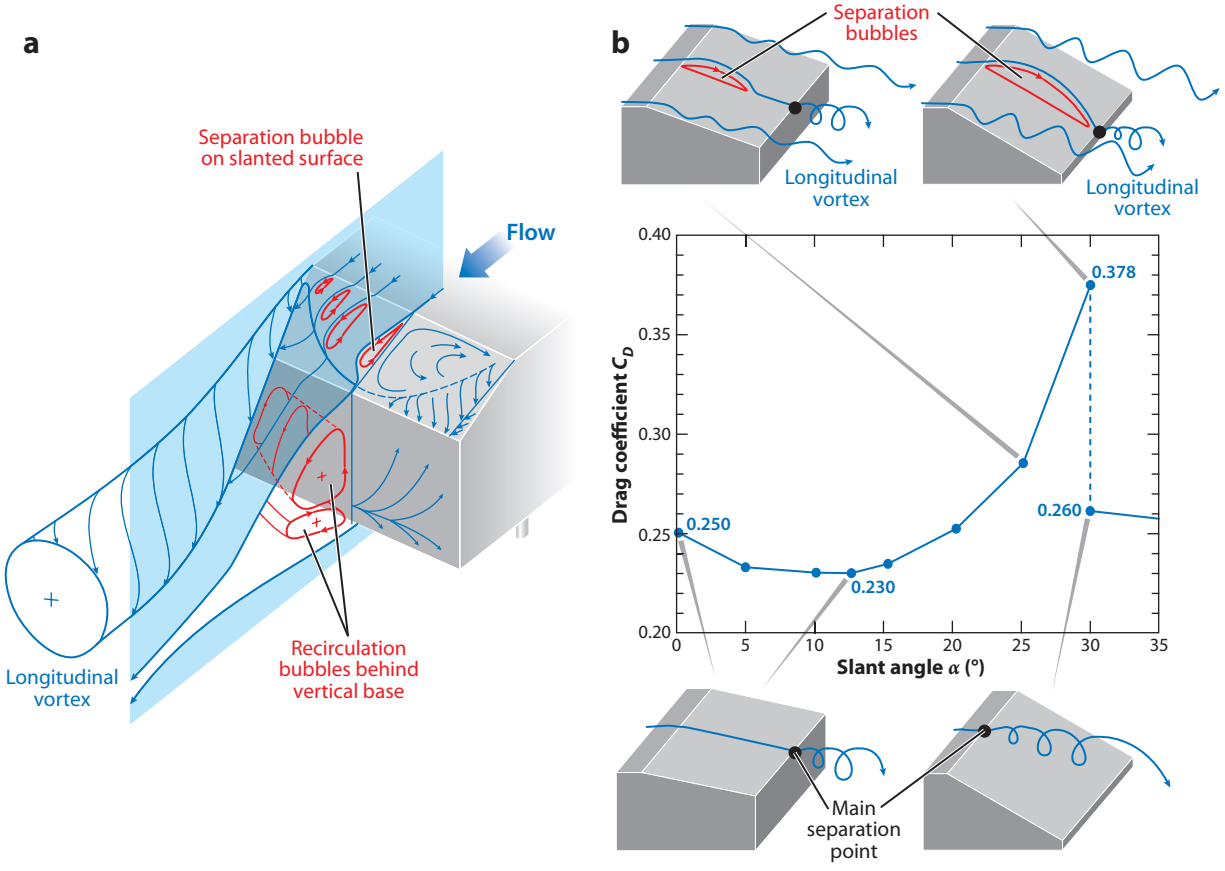

Figure 2

Aerodynamics of the Ahmed model: (*a*) time-averaged three-dimensional flow structures in the wake and (*b*) the drag coefficient (C_D) versus the slant angle (α). In panel *a*, time-averaged streamlines near the slanted surface are shown on the vertical center plane. Panel *b* includes schematic diagrams of the flow patterns at different slant angles. Figure redrawn from Ahmed et al. (1984).

Ahmed et al. (1984) investigated the effect of the rear slant angle (α) on the aerodynamic drag by scrutinizing the time-averaged flow structures in the wake of a model vehicle, where α is defined as the angle between the slanted rear surface and the upper horizontal surface (**Figure 1*a***). In a time-averaged sense, the flow comprises a separation bubble on the slanted surface, a pair of counter-rotating longitudinal vortices emanating from the side edges of the slanted surface, and a recirculation bubble behind the vertical base (**Figure 2*a***). The generation and strength of these flow structures, resulting in drag variation, are governed by the slant angle (α). For $0° < \alpha \leq 12.5°$, the flow remains attached to the slanted surface, and the main separation occurs at its rear edge. In this small-α range, the drag decreases as α increases, and the minimum drag occurs at $\alpha \simeq 12.5°$ (**Figure 2*b***). For $12.5° < \alpha \leq 30°$, the flow separates at the front edge of the slanted surface but quickly reattaches, creating a small recirculating bubble there. The size of this separation bubble increases with the slant angle until it reaches $\alpha = 30°$. In this α range, a pair of counter-rotating longitudinal vortices is generated from the side edges of the slanted surface, and their strength increases with increasing α, becoming the main source of the significant drag increase (called the induced drag) in this range (Hucho & Sovran 1993, Minguez et al. 2008). Interestingly, at the

critical angle of $\alpha = 30°$, regimes of both high and low drag can exist. In the high-drag regime, the strength of the longitudinal vortices reaches a maximum, and the flow separated at the front edge of the slanted surface reattaches right before the vertical base. In the low-drag regime, however, the recirculation bubble on the slanted surface and longitudinal vortices disappear, and fully separated flow develops above the slanted surface. Therefore, the resultant drag is comparable to that with zero slant angle (i.e., $\alpha = 0°$) (**Figure 2*b***).

The unsteady flow structures provide important insights into the vehicle aerodynamics. For example, the flow over the slanted surface of the Ahmed model instantaneously fully separates, even at $\alpha = 25°$, unlike the time-averaged one (Hinterberger et al. 2004, Thacker et al. 2010), and exhibits a separating shear layer over the slanted surface and small-scale vortices in the wake (Krajnović & Davidson 2005a, Minguez et al. 2008). A few studies reported that the dominant frequency of the unsteady motion over the slanted surface at $\alpha = 25°$ is $St_H = fH/u_\infty = 0.25$–$0.3$ (Krajnović & Davidson 2005a, Minguez et al. 2008, Thacker et al. 2010). Minguez et al. (2008) argued that this frequency is related to the instability of the shear layer over the slanted surface. By contrast, Thacker et al. (2010) argued that the frequency may be related to the oscillation of the reattachment position, based on proper orthogonal decomposition analysis. Conversely, the dominant frequency related to the unsteady motion inside the recirculation bubble was measured to be $St_H = 0.3$–0.4 (Minguez et al. 2008, Vino et al. 2005). These studies have not yet provided a full understanding of unsteady flow features.

The GM model is a representative model for square-back ground vehicles and has been used primarily to investigate drag-reduction devices for these vehicles (Han et al. 1996, Khalighi et al. 2001, Verzicco et al. 2002, Yi 2007). The overall geometry of the GM model is similar to that of the Ahmed model with $\alpha = 0°$, but their detailed dimensions differ slightly. The Ahmed model has a variable flow-separation position depending on α, whereas for the GM model, the separation point is fixed at the blunt trailing edge, and thus a large recirculation bubble forms behind the base (**Figure 3*a***) (Lee & Choi 2009). This recirculation bubble is intrinsically

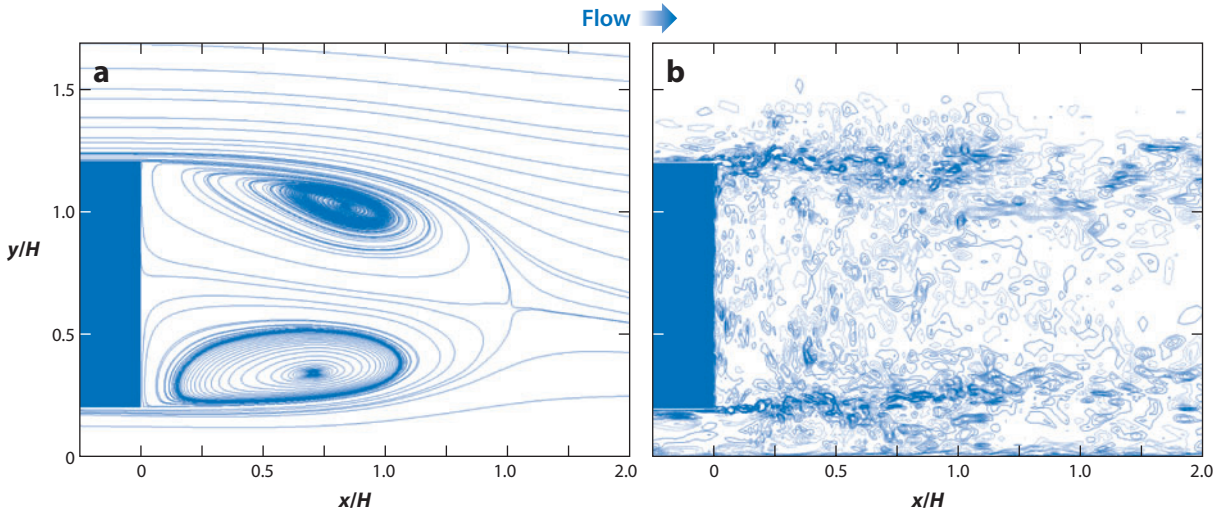

Figure 3

Flow structure in the near wake behind the GM model at the vertical plane of symmetry: (*a*) time-averaged streamlines and (*b*) contours of the instantaneous spanwise vorticity. The flow direction is from left to right. In panel *b*, solid and dashed contour lines correspond to positive and negative vorticity values, respectively. Figure adapted from Lee & Choi (2009).

three dimensional because of the vehicle's geometry, and it causes a significant drop in the base pressure. The control of this recirculation bubble has been the main strategy for drag reduction for square-back vehicles. The counter-rotating longitudinal vortices observed in the near wake of the Ahmed model are not present in the GM model because of the absence of a slanted surface. **Figure 3*b*** shows the instantaneous vorticity contours in the near wake of the GM model (Lee & Choi 2009). The instantaneous flow field exhibits a highly unsteady nature, including a thin shear layer after separation at the trailing edge and small-scale vortices in the wake. The dominant frequency obtained from the velocity signals in the recirculation region or the pressure signals at the model base was $St_H \simeq 0.07$ (Khalighi et al. 2001, Verzicco et al. 2002). It was suggested that this frequency results from the streamwise oscillation of the recirculation bubble behind the model base (Duell & George 1999, Khalighi et al. 2001, Verzicco et al. 2002).

The dynamics of instantaneous flow fields over model vehicles has quite different features from that of time-averaged ones. Despite much effort being devoted to this issue, our current understanding of the unsteady flow characteristics around ground vehicles still lags behind that of the time-averaged flow field. Because the drag-generation mechanism and its control are much more associated with unsteady flow characteristics (Choi et al. 2008), a more systematic analysis on unsteady flow features is required.

2.1.2. Ground effect. When a moving bluff body is placed near a wall, the wall's proximity has a significant effect on the aerodynamic forces and flow structure, and this has been referred to as the ground effect. Therefore, the importance of using a proper ground condition has been emphasized in ground vehicle aerodynamics research; for example, the flow around a vehicle (Fago et al. 1991, Hucho & Sovran 1993, Krajnović & Davidson 2005c, Strachan et al. 2007) and the performance of drag-reduction devices (Geropp & Odenthal 2000, McCallen et al. 2005, Siewny et al. 2010) vary noticeably depending on the type of ground. Krajnović & Davidson (2005c) investigated the effects of the ground condition on the flow around the Ahmed model at $Re_H = 2 \times 10^5$ using large-eddy simulation (LES), in which the ground clearance (C) is $C/H = 0.174$. They showed that the vehicle experiences lower drag by 8% and lift by 16% with a moving ground than with a stationary ground. It was also found that the flow in the wake has a dominant peak frequency in the power spectral density with a moving ground, whereas the power spectral density is more scattered in the case of a stationary ground. The influence of a moving ground was limited to the near-wake region between the ground and the shear layer separating from the vehicle underbody. Strachan et al. (2007) also experimentally measured the velocity field around the Ahmed model with a moving ground at $Re_H = 4.7 \times 10^5$. They reported that the moving ground causes secondary vortices to appear between the ground and underbody, which was not observed in the case of a stationary ground, but their effect on aerodynamic performance, such as the drag, was not investigated. Siewny et al. (2010) performed a Reynolds-averaged Navier-Stokes (RANS) simulation to investigate the effect of ground clearance on the performance of a time-periodic blowing/suction at the base of a two-dimensional generic truck model with a moving ground ($Re_H = 9.24 \times 10^5$) and showed that the amount of drag reduction is reduced as the ground clearance decreases.

Only a few studies have investigated the ground effect for heavy vehicles. Allan (1981) measured the drag acting on two three-dimensional rectangular bodies moving in tandem (a simplified tractor-trailer) with a moving ground at $Re_H = 5.1 \times 10^5$ and showed that the drag increases as the ground clearance increases. Barlow et al. (2001) measured the drag on a rectangular body (with various aspect ratios) with a stationary ground by varying the ground clearance at $Re_H = 1.9 \times 10^6$. They also showed that the drag increases with increasing ground clearance, and this effect becomes stronger as more underbody area is exposed to the ground. Using LES, Ortega et al. (2004) showed

that a massively separated flow behind a tractor-trailer at $Re_H = 2.8 \times 10^6$ interacts with a stationary ground, creating a secondary separation bubble on the ground.

The ground clearance (C) of typical heavy vehicles is $C/W = 0.36$–0.50 for tractor-trailers (Allan 1981, Storms et al. 2004) and 0.08–0.16 for buses (Fletcher & Stewart 1986, Krajnović & Davidson 2003) and is much larger than that of a typical racing car (0.005; Zhang et al. 2006) or passenger car (0.03; Geropp & Odenthal 2000), where W is the spanwise width of the vehicle. High ground clearance implies that the ground effect may not be important for heavy vehicles; instead, large flow structures existing in the ground clearance (e.g., flow separation from rolling tires) interact with the vehicle underbody, working as a nonnegligible source of aerodynamic drag. For example, a rotating exposed tire, in the presence of the ground, generates a pair of counter-rotating longitudinal vortices behind it (McManus & Zhang 2006, Mercker & Bernerburg 1992, Pirozzoli et al. 2012). When a tire is enclosed by a wheelhouse, vortices are induced at the side of the tire owing to the outward deflection of the flow entering into the wheelhouse (Regert & Lajos 2007). The rolling tire aerodynamics itself also has important practical implications for the aerodynamic design of ground vehicles, as the drag associated with rolling tires is responsible for up to 25% of the total aerodynamic drag of a passenger car (Wickern et al. 1997). In the case of a tractor-trailer, in which the tires are not enclosed, additional drag is expected because of the interaction between the separating flow and the trailer underbody (Sreenivas et al. 2006); however, detailed experimental and numerical data are needed to fully understand and control the interaction. Finally, the splash and spray of water thrown by a heavy vehicle on a wet road, caused by the interaction between rolling tires and the ground, have been raised as important issues for the safety of adjacent vehicles and pedestrians passing nearby (Gotz & Mayr 1998, Hucho & Sovran 1993, Paschkewitz 2006), and this also needs to be investigated in detail in future research.

2.2. Flow Around a Tractor-Trailer

Geometrically, a tractor-trailer consists of two rectangular bluff bodies moving in tandem near the ground; thus, the flow structure around it has interesting features, such as multiple stagnation points, gap flow, underbody flow, and a large wake region, all of which contribute to the aerodynamic drag (Buil & Herrer 2009, Cooper 2003, Wood 2006, Wood & Bauer 2003). In this section, we discuss the flow around a tractor-trailer, mainly focusing on flow structures around the simplified models shown in **Figure 4**. Various drag-reduction devices to control these flow structures are discussed in Section 3.

Two simplified tractor-trailer models were developed in a multiyear research project (McCallen et al. 2004b) by the Heavy Vehicle Aerodynamic Drag Consortium to obtain a clear understanding of the flow phenomena responsible for aerodynamic drag. Since then, many studies have investigated their aerodynamics using experimental and computational approaches. The two models are the ground transportation system (GTS) (Croll et al. 1996, Gutierrez et al. 1996, Maddox et al. 2004, McCallen et al. 2004b, Ortega et al. 2004, Roy et al. 2006, Salari et al. 2004, Storms et al. 2001) and the generic conventional model (GCM) (Heineck et al. 2004, Hyams et al. 2011, McCallen et al. 2004b, Paschkewitz 2006, Storms et al. 2004). The GTS is the most simplified version. In this system, the tractor and trailer are combined smoothly without any real geometric features, whereas the GCM is more realistic in terms of the gap between the tractor and trailer and the streamlined tractor shape (**Figure 4**). In both the GTS and GCM configurations, no undercarriage of the tractor or trailer is present (i.e., a flat, smooth surface is applied instead). Later, more realistic modifications were applied to

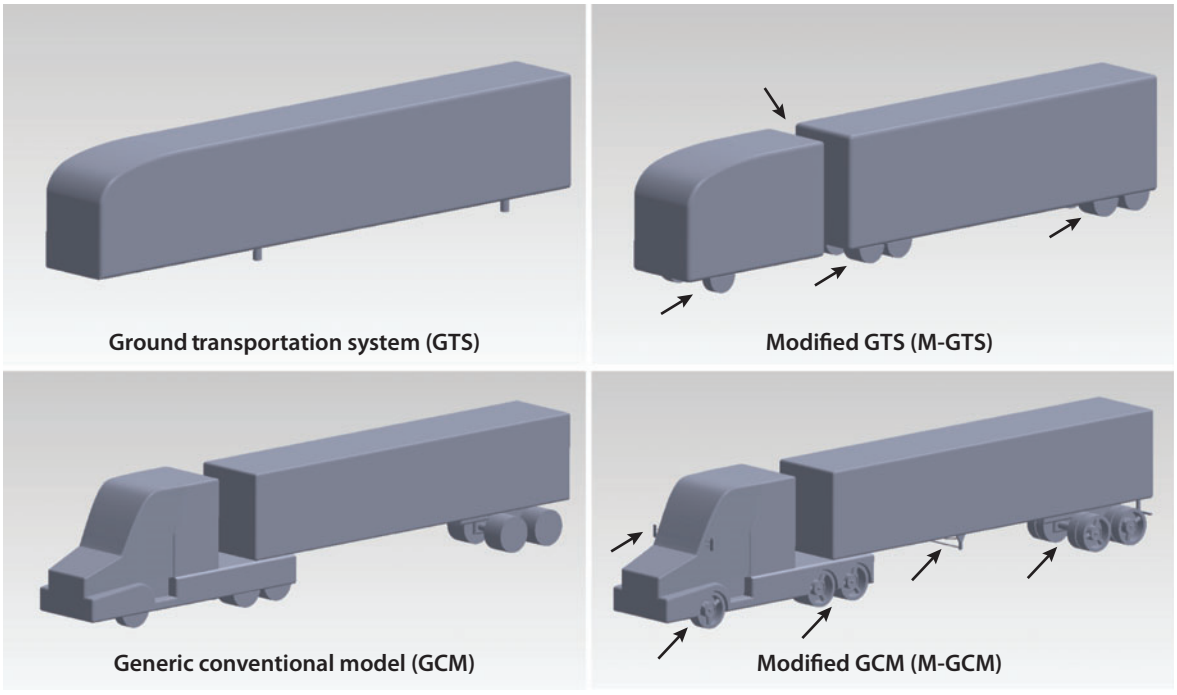

Figure 4

Simplified tractor-trailer models: ground transportation system (GTS), generic conventional model (GCM), and their modifications (M-GTS and M-GCM). The modifications for the M-GTS and M-GCM are highlighted with arrows. Figure redrawn from Salari (2006).

these models to make the modified ground transportation system (M-GTS) (Castellucci & Salari 2005, McCallen et al. 2005) and the modified generic conventional model (M-GCM) (**Figure 4**). In addition, Buil & Herrer (2009) performed a numerical simulation to investigate the flow around a tanker with a cylindrical load instead of a rectangular trailer and showed that its flow characteristics are similar to those around a typical tractor-trailer.

Generally, the flow around a tractor-trailer model under the no-crosswind (zero yaw angle) condition stagnates near the front grill of the tractor and separates at the trailing edge of the tractor body, forming counter-rotating vortices trapped inside the gap between the tractor and the trailer (except in the GTS, which lacks such a gap). The flow above the surface of the trailer body remains attached and then separates at its trailing edge, resulting in a large wake (**Figure 5**). We note that the flow structures shown in this figure should be understood only qualitatively because no information on numerical accuracy was given in these computations. This overall picture of the flow was confirmed by static surface pressure measurements along the center line of the tractor-trailer: Along the upper surface of the vehicle, the surface pressure drops significantly in the gap and then recovers, approaching the free-stream condition as the flow goes downstream to the trailing edge of the trailer (Croll et al. 1996, Gutierrez et al. 1996, Maddox et al. 2004, Roy et al. 2006, Salari et al. 2004).

The gap flow between the bodies of the tractor and trailer is an important flow feature affecting fuel consumption and driving stability. Many experimental and computational studies have examined this flow (Castellucci & Salari 2005, Hammache & Browand 2004, Heineck et al. 2004, Hyams et al. 2011, Malviya et al. 2009, Östh & Krajnović 2012, Storms et al. 2004). Hammache

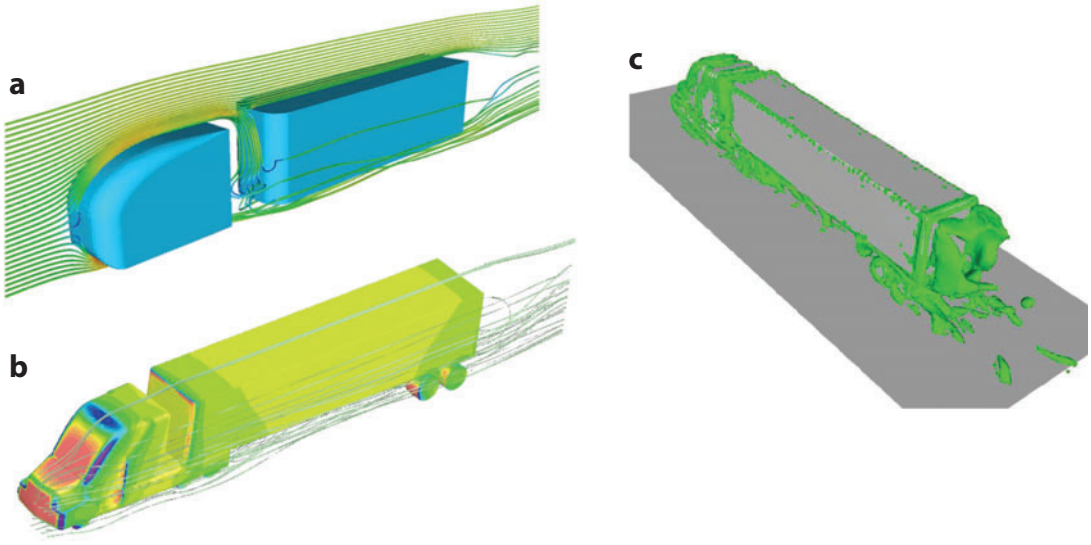

Figure 5

Flows around simplified tractor-trailer models simulated by Reynolds-averaged Navier-Stokes (RANS). (*a*) Particle traces around the modified ground transportation system (M-GTS) colored by the velocity magnitude. (*b*) Streamlines around the generic conventional model (GCM) with the surface pressure distribution. Red denotes the positive pressure, and blue denotes the negative pressure. Panels *a* and *b* taken from McCallen et al. (2004b). (*c*) Vortical structures [isosurfaces of $Q = 100$, where Q denotes the Q criterion by Hunt et al. (1988)] around the GCM predicted by unsteady RANS. Panel *c* taken from Paschkewitz (2006).

& Browand (2004) showed experimentally that the gap flow and the resulting influence on the drag (mostly focusing on the drag on the trailer body) vary greatly depending on the gap clearance and yaw angle. For example, at $0.1 \lesssim G/\sqrt{A} \lesssim 0.5$, the drag force on the trailer (and the total drag force on the tractor-trailer) shows a minimum plateau (**Figure 6*a***), where G is the gap distance and A is the frontal area of the vehicle. In this regime, the gap flow consists of symmetric, counter-rotating vortices, which are generally steady, resulting in a low-pressure region at the front face of the trailer and drag reduction (**Figure 6*b***). When the gap becomes smaller ($G/\sqrt{A} < 0.1$), the pressure inside the gap increases, which increases both the base pressure on the tractor (drag reduction) and the frontal face pressure on the trailer (drag increase). When the gap distance increases beyond the critical value ($G/\sqrt{A} > 0.5$–0.6), flow symmetry breaks down, and unsteady flow separation occurs intermittently at the trailing edge of the tractor. This flow structure significantly increases the drag on the trailer, while this trend is maintained up to $G/\sqrt{A} \simeq 0.8$ and then saturates. Castellucci & Salari (2005) also showed that the drag force on the M-GCM increases substantially when $G/\sqrt{A}$ increases from 0.35 to 0.65 at a yaw angle (β) of 6°. At low yaw angles, the effect of the gap distance on the drag force is large; however, the increase in drag with increasing gap distance is not significant at high yaw angles ($\beta \geq 10°$). Interestingly, it has been noted that the value of $G/\sqrt{A}$ of the GCM is 0.35, which provides minimum drag (**Figure 6*a***) and is within the range of real tractor-trailer configurations.

Without any add-on devices or shape modification, the separation point is generally fixed at the trailing edge of the trailer body, and there is a large wake region with a significant pressure drop. Many studies have tried to establish a clear understanding of this wake flow (Croll et al. 1996, Gutierrez et al. 1996, McCallen et al. 2004b, Ortega et al. 2004, Raemdonck & Tooren 2009, Roy et al. 2006, Salari et al. 2004). Investigations of instantaneous flow fields have shown

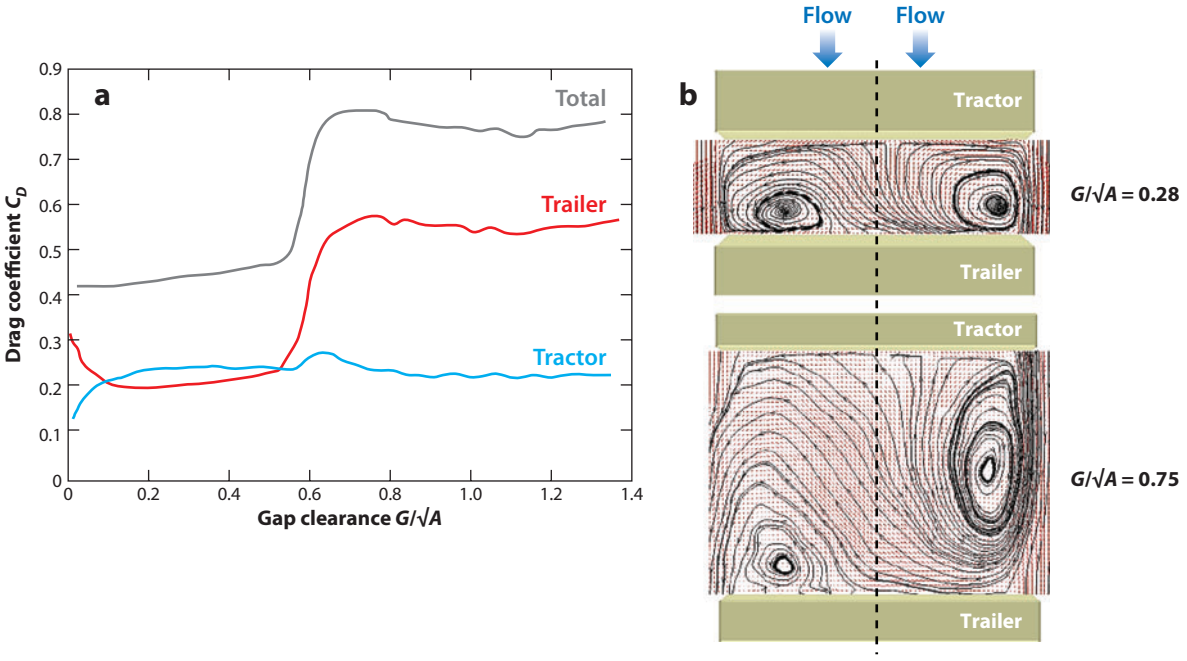

Figure 6

Flow in the gap between the tractor and trailer: (*a*) drag coefficients versus gap clearance ($G/\sqrt{A}$) and (*b*) the time-averaged flow structure in the gap at $G/\sqrt{A} = 0.28$ and 0.75 (top view). Figure redrawn from Hammache & Browand (2004).

that separating shear layers develop at the trailing edges of the trailer. These shear layers roll up into vortex rings that advect downstream but break shortly afterward, or extend downstream and undulate periodically while shedding patches of vorticity (Ortega et al. 2004). From the time-averaged flow, a large recirculation bubble is found in the wake (Croll et al. 1996, Gutierrez et al. 1996, McCallen et al. 2004b, Ortega et al. 2004, Roy et al. 2006, Salari et al. 2004), resembling those in the wake flow behind the GM model (see Section 2.1.1). However, there is some data scatter in the location and strength of this recirculation bubble in the experimental and computational results, possibly because of the geometry truncation, boundary condition, grid resolution, and turbulence models adopted by numerical studies.

During real operations, a tractor-trailer is often under the influence of a crosswind; in other words, the streamwise body axis has a certain yaw angle against the wind direction, substantially affecting the aerodynamic forces and stability of the vehicle (Hyams et al. 2011, McCallen et al. 2004b, Salari et al. 2004). The crosswind causes a flow separation at the frontal edge of the tractor body that evolves into A-pillar vortices, and the separated flow reattaches to the leeward side of the tractor body, forming a separation bubble (Maddox et al. 2004, Salari et al. 2004) (**Figure 7**). The crosswind also increases the velocity and volume of the flow entering the gap and impinging on the frontal face of trailer and causes high pressure there. This also reduces the base pressure on the tractor body and thus increases the drag on the tractor. The flow through the gap separates from the leeward side of the trailer and produces a significant side force on the vehicle, which may have an adverse effect on vehicle handling (Wood & Bauer 2003). As discussed in Section 2.1.2, the relatively large clearance between the ground and underbody structures such as the axles and wheels causes the flow under the trailer to be highly separated and turbulent,

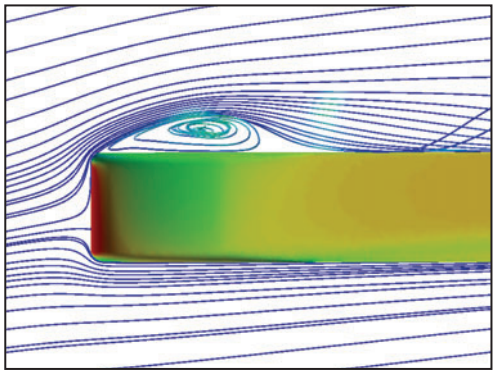

Figure 7

Flow around the ground transportation system (GTS) at a yaw angle of 10° predicted from detached-eddy simulation. Shown here are the time-averaged streamlines (top view). Figure reproduced from Maddox et al. (2004).

resulting in a large drag force (Raemdonck & Tooren 2009). Furthermore, the crosswind makes the underbody flow more complex and increases both drag and side forces (Buil & Herrer 2009, McCallen et al. 2004b, Mohamed-Kassim & Filippone 2010, Ortega & Salari 2004, Storms et al. 2004).

2.3. Flow Around a Bus

A bus is a representative square-back ground vehicle, and its aerodynamic features are similar to those of the GM model. In general, a bus has rounded edges that are known to enhance aerodynamic performance (Cooper 1985, Hucho et al. 1976, Krajnović & Davidson 2003). Cooper (1985) investigated the effect of front-edge roundness on the flow around a bus-shaped model vehicle and showed that the effect of front-edge roundness ($r/\sqrt{A}$) on the aerodynamic performance is strongly influenced by the Reynolds number Re_A ($\equiv u_\infty \sqrt{A}/\nu$), where r is the radius of the front edge, and A is the frontal area of the vehicle. That is, at a fixed $r/\sqrt{A}$, the drag rapidly decreases and then remains constant with increasing Re_A. The transcritical Reynolds number (i.e., the Reynolds number after which the drag remains constant; e.g., $Re_{A,\mathrm{trans}} = 1.32 \times 10^6$ for $r/\sqrt{A} = 0.1$) decreases with increasing $r/\sqrt{A}$. Below the transcritical Reynolds number, the flow separates at the front edge and then reattaches, forming a separation bubble on the vehicle surface; above the transcritical Reynolds number, the flow becomes fully attached to the surface. These results are informative for designing a bus-shaped vehicle. For example, the front-edge roundness of a bus should be $r/\sqrt{A} \geq 0.125$ to obtain low drag without flow separation at the front edge in $Re_A \geq 10^6$ (Cooper 1985).

2.4. Flow Around a High-Speed Train

In Asia and Europe, HST systems with maximum speeds above 300 km h^{-1} are being widely operated, and thus there is a rapidly growing need to improve their performance or to develop new HSTs (Raghunathan et al. 2002). Many issues important to the aerodynamics of HSTs, such as the aerodynamic noise and vibration, the interaction between two trains passing each other, and the occurrence of an impulse wave at the exit of a tunnel, have also received much attention (Auvity et al. 2001, Baker 2010a, Hemida & Krajnović 2008, Raghunathan et al. 2002, Schetz

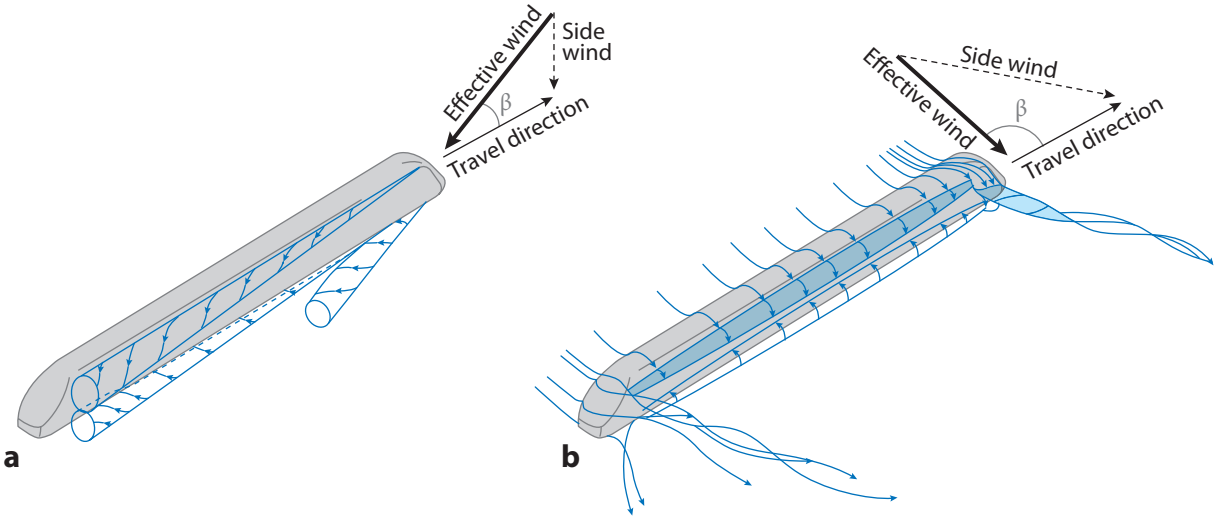

Figure 8

Schematic diagrams of the flow around a high-speed train under a crosswind: (*a*) at small and moderate yaw angles and (*b*) at a high yaw angle. Figure redrawn from Khier et al. (2000).

2001). Although HSTs share many operating conditions with other ground vehicles, they exhibit some special flow features that we briefly address here [for details, see reviews by Ahmed et al. (1985), Baker (2010a), Raghunathan et al. (2002), and Schetz (2001)].

The most obvious difference between HSTs and other ground vehicles is the large contribution of the skin friction to the total aerodynamic drag force because of the much higher length-to-width ratio of trains relative to other ground vehicles (Schetz 2001). The high speed, large length-to-width ratio, and relatively low weight of an HST indicate that the flow around it causes significant instability when the train is under a strong crosswind (Baker 2010b, Hemida & Krajnović 2008, Khier et al. 2000, Raghunathan et al. 2002, Schetz 2001) or when trains are passing each other (Hwang et al. 2001, Raghunathan et al. 2002).

When an HST is under a crosswind effect, flow separation takes place at both the lower and upper leeward edges. The vortical structures emanating from these edges depend on the yaw angle (β) (**Figure 8**). No flow separation at the edges of the windward side is observed. At small and moderate β's, a pair of streamwise vortices originates from the upper and lower leeward edges of the train nose, and they grow steadily along the axial direction and interact with each other (**Figure 8*a***). When β is large, flow separation occurs along the entire upper and lower edges of the leeward side of the train, and secondary vortices are generated at the leading and trailing noses (**Figure 8*b***) (Baker 2010a, Khier et al. 2000). Hemida & Krajnović (2008) performed an LES with good resolution at $Re_H = 3 \times 10^5$ to investigate the effect of the nose shape (short and long noses) on the flow around an HST at $\beta = 90°$. For the short-nose model, a small separation bubble is formed on the roof and leeward surfaces near the nose, but for the long-nose model, the flow remains attached along most of the roof and leeward surfaces. When two trains pass each other, three-dimensional unsteady impulse forces are generated, resulting in unfavorable periodic pushing and pulling side forces. That is, a positive-negative pulse pressure is imposed on the side surface of a train when the forebody of the train passes by another train, while a negative-positive pulse is generated as the afterbody passes by. This phenomenon is mainly governed by the movement of the stagnation pressure point at the nose and also by a

lower-pressure region near the shoulder of the train (Raghunathan et al. 2002). Therefore, an optimal design of the nose shape can effectively control the strong side force and yawing moment under a crosswind or when two trains are passing each other (Cheli et al. 2010).

When an HST enters a tunnel, the high entry speed and the large blockage ratio between the train and the tunnel cross-sectional area produce important aerodynamic phenomena that do not exist with other ground vehicles (Baker 2010a, Bourquin et al. 2004, Mok & Yoo 2001, Raghunathan et al. 2002, Ricco et al. 2007, Schetz 2001). When an HST enters a tunnel, a compression wave is generated in front of the train and propagates along the tunnel. At the tunnel exit, the compression wave is reflected back into the tunnel, forming an expansion wave. These pressure waves cause additional aerodynamic forces and moments on the train (this aerodynamic drag can exceed 90% of the total drag on a train when passing through a tunnel) and on facilities inside the tunnel. Furthermore, such waves can cause serious discomfort for passengers. The strength of the compression wave depends mainly on the blockage ratio and entry speed of an HST; by contrast, the cross-sectional shape of the train does not have a significant influence on wave generation (Ricco et al. 2007). Auvity et al. (2001) investigated the flow at a tunnel exit influenced by the entry of an HST and showed that the mass of the ejected jet flow is approximately 20% of the compressed air inside the tunnel at low speed but is comparable to the total mass of compressed air inside the tunnel at high speed. This jet flow at the tunnel exit is considered an environmental disturbance to residents nearby.

3. DRAG-REDUCTION DEVICES FOR HEAVY VEHICLES

In this section, we discuss various drag-reduction devices for heavy vehicles, mostly tractor-trailers. Studies on drag reduction for simplified model vehicles (the Ahmed and GM models) are also discussed. We classify the devices as those for forebody, base, and underbody drag reduction, depending on the locations on the vehicle at which they are applied.

3.1. Forebody Drag Reduction

Various attempts have been made to reduce the forebody drag, where the forebody refers to the tractor of a tractor-trailer (including the gap between it and the trailer) or to the nose shape of a bus or HST. For a typical tractor-trailer operating on a highway, approximately 45% of the aerodynamic drag comes from the flow structures existing at the front face of the tractor (25%) and the gap (20%) between the tractor and trailer (Wood 2006). So far, many devices have been suggested for forebody drag reduction, but a few are actually being used widely by truck fleet operators. The earliest attempt to enhance fuel economy through drag reduction was to increase the radius of all the front corners and edges of a tractor and to add a smooth fairing to the tractor roof. With these modifications, Steers & Saltzman (1977) reported approximately 20% fuel savings from a full-scale test on a highway. Later on, many add-on devices were developed to control the flow around the tractor body. These include (*a*) a vertical fence on the tractor roof (Allan 1981), a cap deflector/roof fairing (Cooper 2003, Leuschen & Cooper 2009, Malviya et al. 2009), and moving surface boundary-layer control (Malviya et al. 2009) to create a more streamlined flow passage from the stagnation point to the trailer and (*b*) a front spoiler under the tractor (Hyams et al. 2011, Pankajakshan et al. 2009) to reduce the flow velocity in the underbody region. The typical shapes and positioning of these devices are shown in **Figure 9*a***.

Another strategy for forebody drag reduction is to control the gap flow (**Figure 9*b***), which includes a gap enclosure (Allan 1981, Muirhead & Saltzman 1979), cab side extender (Castellucci & Salari 2005, Cooper 2003, Hyams et al. 2011, Storms et al. 2004), splitter plate at the frontal face of a trailer (Castellucci & Salari 2005, Hyams et al. 2011, McCallen et al. 2004b,

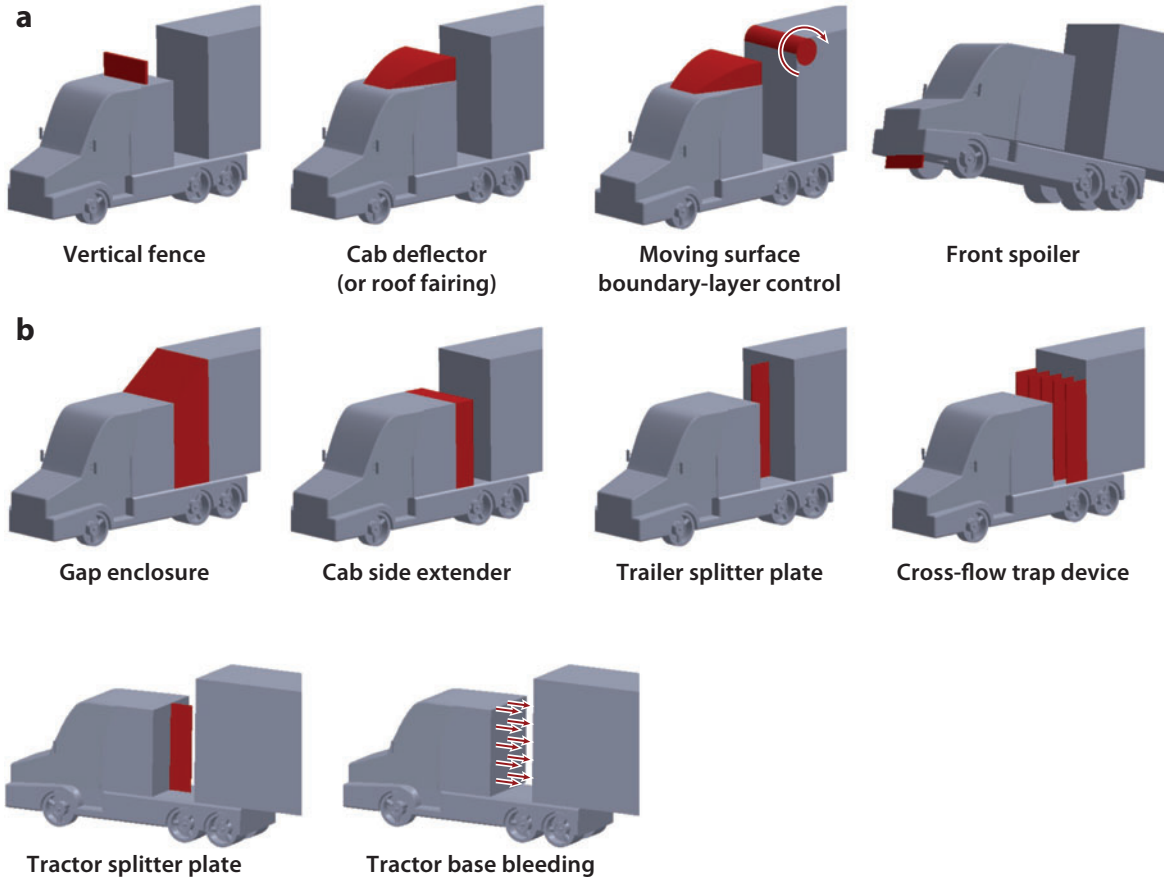

Figure 9

Devices and positioning for forebody drag reduction of a tractor-trailer. (*a*) Forebody flow control: vertical fence, cap deflector, moving surface boundary-layer control, and front spoiler. (*b*) Gap flow control: gap enclosure, side extender, trailer splitter plate, cross-flow vortex trap device, tractor splitter plate, and tractor base bleeding.

Mohamed-Kassim & Filippone 2010), cross-flow vortex trap device (Wood 2006, Wood & Bauer 2003), splitter plate at the base of a tractor (Cooper 2003), and tractor base bleeding (Ortega et al. 2007). Among these, the side extender is one of the most widely used add-on devices to reduce the gap flow. It delays the flow separation at the tractor, thus pushing the low-pressure region away from the tractor base and reducing the drag. As the reduced flow volume impacts the frontal surface of the trailer, the drag force on a trailer also decreases (Castellucci & Salari 2005). The splitter plate at the frontal face of a trailer has also been proposed to interfere with the gap flow, but it is not as effective as the side extender (Castellucci & Salari 2005, Hyams et al. 2011). The splitter plate at the base of a tractor has been shown to block the gap flow at large yaw angles to reduce the drag force (Cooper 2003). Wood (2006) and Wood & Bauer (2003) installed multiple vertical splitter plates (a cross-flow vortex trap device) at the frontal face of a trailer. As the cross flow develops in the gap, it separates at the leading edges of the splitter plates and forms a vortex trapped between the plates. These trapped vortices locally induce low pressure, thereby reducing the drag force on the trailer. They estimated that up to 10% fuel savings could be obtained with the vortex trap device. Ortega et al. (2007) investigated the effect of base bleeding on the gap flow and claimed

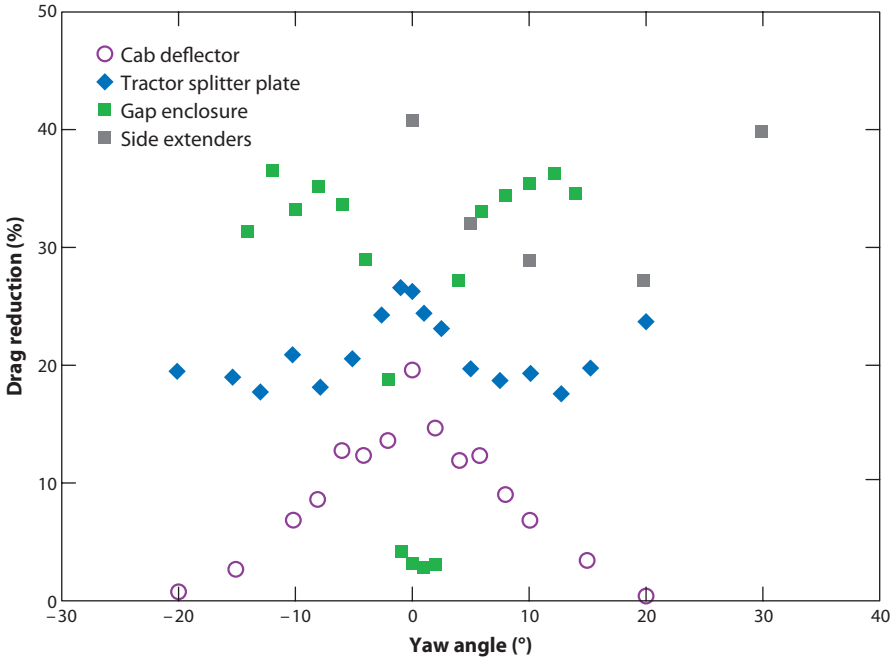

Figure 10

Magnitude of drag reduction (by percentage) versus the yaw angle: for a cab deflector (*purple circles*) (Cooper 2003), tractor splitter plate (*blue diamonds*) (Cooper 2003), gap enclosure (*green squares*) (Muirhead & Saltzman 1979), and side extenders (*gray squares*) (Storms et al. 2004).

that base bleeding achieves more drag reduction than side extenders. However, base bleeding requires an additional cost of implementing an active bleeding system and also an operation cost.

Because a tractor-trailer is operated mostly in open areas (e.g., on highways), its aerodynamics varies significantly under crosswind conditions, and thus the performance of an add-on device for drag reduction needs to be assessed at various yaw angles (**Figure 10**). As shown in the figure, the yaw angle significantly affects the performance of drag reduction. For example, the cab deflector (or roof fairing) produces the largest drag reduction (approximately 20%) at a yaw angle of zero, but the amount of drag reduction decreases with increasing yaw angle. The behavior of drag reduction by the tractor splitter plate is in general similar to that of the cab deflector, but the amount of drag reduction by the former is bigger than that of the latter. At large yaw angles (e.g., $\beta \geq 15°$), the amount of drag reduction (by percentage) by the tractor splitter plate increases. This nonmonotonic behavior should also be associated with the length of the splitter plate, which needs to be investigated further. The behavior of drag reduction by the gap enclosure is opposite to that of the cap deflector and tractor splitter plate; in other words, the percentage of drag reduction is minimum at $\beta = 0°$ and increases rapidly with increasing $|\beta|$, reaching more than 30% at $|\beta| \gtrsim 5°$. The reason for this increase in drag reduction is currently not clear and needs to be investigated. The behavior of drag reduction by the side extender is similar to that of the gap enclosure, except that the percentage is minimum at $\beta \simeq 20°$, although its magnitude is already big enough ($\geq$20%). Again, the detailed mechanism for the change in drag is not clear.

Along with these add-on devices, optimizations of the nose shapes of HSTs (Cheli et al. 2010, Herbst et al. 2009, Krajnović 2009) and buses (Krajnović et al. 2009) have been examined. It was

shown that the lateral force and rolling moment are reduced at large yaw angles ($\beta \geq 40°$) by optimizing the nose shape of the vehicle.

3.2. Base Drag Reduction

Because most heavy vehicles have bluff-body shapes with blunt trailing edges, the contribution to the drag from the pressure drop at the base is large (Hucho & Sovran 1993). For a typical tractor-trailer operating on a highway, approximately 25% of the aerodynamic drag comes from the trailer base (Wood 2006), and much effort has been devoted to base drag reduction for heavy vehicles. Here, we discuss various approaches to reduce base drag for fast-back and square-back vehicles that have slanted and blunt trailing edges, respectively.

3.2.1. Base drag reduction for fast-back heavy vehicles. As discussed in Section 2.1.2 (see also **Figure 2*b***), the separation bubble on the slanted surface and a pair of counter-rotating longitudinal vortices are the major sources of the substantial increase in drag on the Ahmed model at slant angles of $12.5° < \alpha \leq 30°$. Thus, various ways to weaken or eliminate these flow structures have been examined to reduce the base drag on the Ahmed model (**Figure 11*a***).

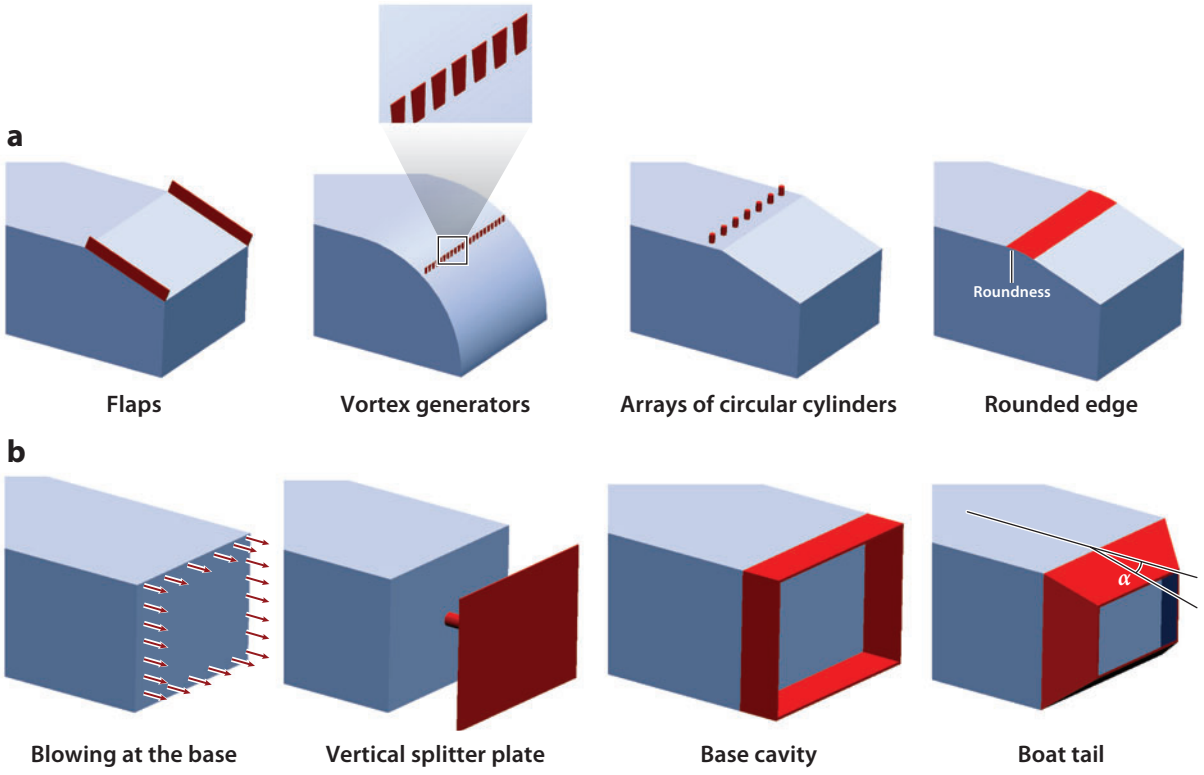

Figure 11

Devices for base drag reduction. (*a*) Fast-back heavy vehicle control: flaps, vortex generators, an array of circular cylinders, and a rounded edge. (*b*) Square-back heavy vehicle control: blowing at the base, a vertical splitter plate, a base cavity, and a boat tail with slant angle (α).

One way to reduce the drag on the Ahmed model is to make the flow fully attached on the slanted surface by eliminating the local separation bubble on it. Pujals et al. (2010) installed an array of small, circular cylinders on the roof slightly ahead of the slanted surface ($\alpha = 25°$) and found that it attaches the flow on the slanted surface, resulting in drag reduction. They demonstrated that these three-dimensional protrusions generate coherent streamwise vortices that prevent the formation of a separation bubble on the slanted surface by promoting high-momentum flow near the wall. Thacker et al. (2012) showed that rounding the edge between the roof and the slanted surface ($\alpha = 25°$) also prevents flow separation from the slanted surface and reduces the drag by 10%.

Another way to reduce the drag on the Ahmed model is to attenuate the strength of the longitudinal vortices by making the flow fully separated from the front edge of the slanted surface. With this control, the controlled flow field is similar to that in the low-drag regime at the critical slant angle $\alpha = 30°$ (**Figure 2*b***). Beaudoin & Aider (2008) showed that flaps attached to the side edges of a slanted surface of a modified Ahmed model ($\alpha = 30°$) effectively interrupt the flow from reattaching to the slanted surface and induce it to fully separate, preventing the generation of longitudinal vortices. Interestingly, this approach intentionally encourages early massive separation to achieve drag reduction, which goes against the conventional wisdom in aerodynamics research that delaying massive separation is favorable for low drag. A similar mechanism was realized by Aider et al. (2010), who examined the effect of vortex generators installed near the main separation point on the flow over a modified Ahmed model having a curved rear body surface. Contrary to their conventional function, the vortex generators did not delay flow separation, but rather triggered early separation and induced a very large recirculation bubble, by which the formation of longitudinal vortices was prevented, resulting in drag reduction.

3.2.2. Base drag reduction for square-back heavy vehicles. For flow over a square-back vehicle such as the GM model, the most distinguished feature is that the flow separation is fixed at the blunt trailing edge, and a large recirculation bubble is formed in the wake. This recirculation bubble is responsible for the drop in base pressure. Thus, base drag reduction has been achieved by reducing the size of this bubble or by shifting it further away from the base (Balkanyi et al. 2002, Englar 2001, Gilliéron & Kourta 2010, Howell et al. 2003, Littlewood & Passmore 2012, Peterson 1981, Wong & Mair 1983, Yi 2007). Successful control devices based on this mechanism are the blowing at the base, vertical splitter plates, base cavities, and boat tails (**Figure 11*b***).

The blowing at the base, including base bleeding, achieves drag reduction by pushing the low-pressure region downstream (Englar 2001, Howell et al. 2003, Littlewood & Passmore 2012). However, the additional power input required to provide blowing is relatively high, and thus its practical use has been limited. Gilliéron & Kourta (2010) showed that a vertical splitter plate located in the near wake behind the base of the Ahmed model with $\alpha = 0°$ interrupts the formation of a recirculation bubble, resulting in drag reduction. However, its installation on a heavy vehicle is impractical because of the large size of the plate.

Base cavities and boat tails have been considered the most effective and practical devices for base drag reduction. A base cavity consists of four downstream extensions from the edges of the base that together form a cavity, whereas a boat tail is a tapering extension with a slant angle (α) from the edges of the base. Both devices push the recirculation bubble downstream, and/or reduce its size by delaying the main flow separation or by deflecting the main flow inward from the trailing edge of the main body (Balkanyi et al. 2002, Khalighi et al. 2001, Verzicco et al. 2002, Yi 2007). Peterson (1981) showed that a truncated boat tail (made by cutting off a portion of a full boat tail) has the same performance of drag reduction as that of a full boat tail that forms an apex at the rear end. Balkanyi et al. (2002) investigated the effect of the geometries of the base cavity and truncated boat tail on the aerodynamics of the GM model; more drag reduction is achieved when the base

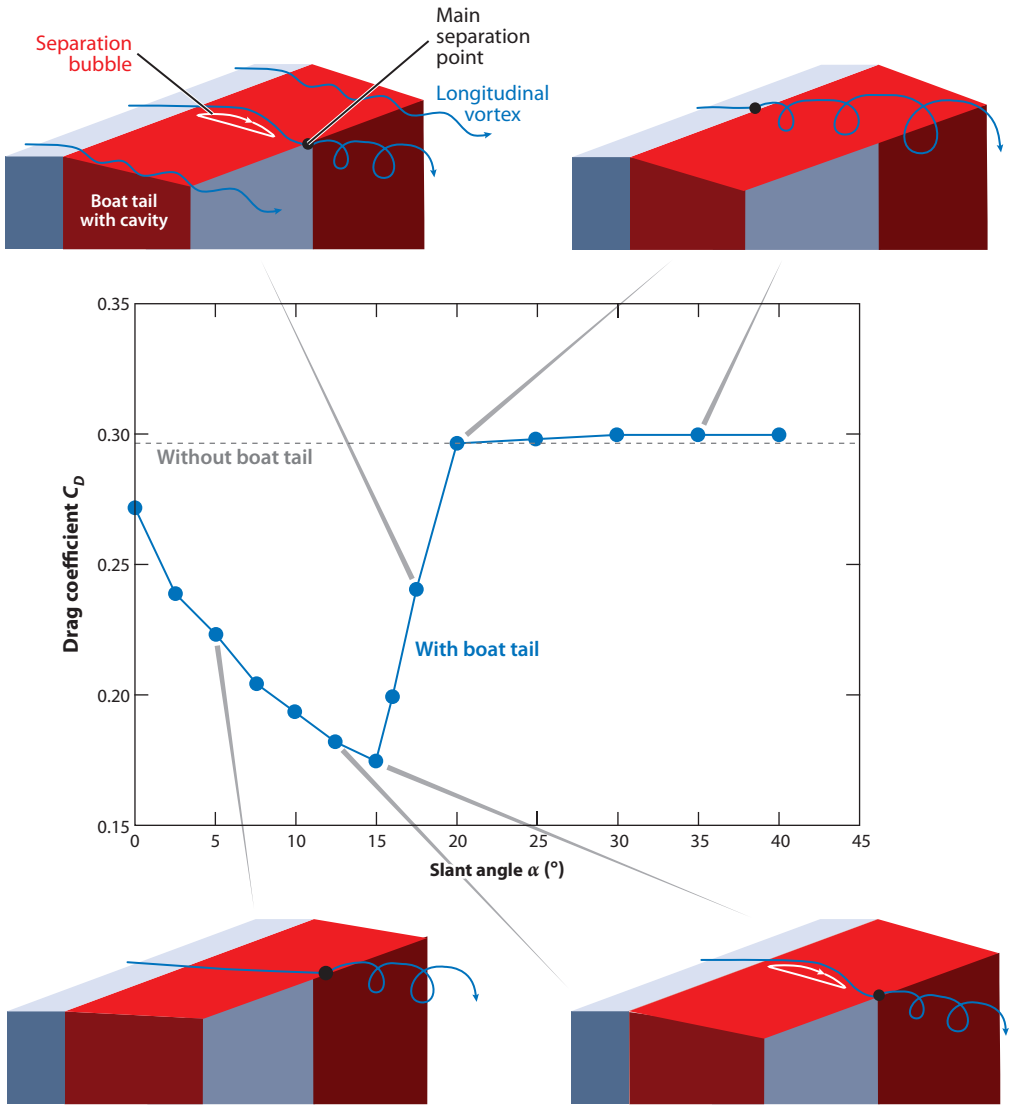

Figure 12

Variation of the drag coefficient (C_D) of the GM model with the slant angle (α) of the boat tail. Schematic diagrams of flow patterns are also shown on the vertical center plane. Figure taken from Yi (2007).

cavity is offset inward, and boat tails with a cavity perform better than those without. Moreover, the length and slant angle of the boat tail strongly affect the drag-reduction performance (Han et al. 1992, Wong & Mair 1983, Yi 2007). Yi (2007) investigated the effect of the boat-tail geometry (by varying α) on the flow structure near the boat tail and the drag of the GM model (**Figure 12**). He suggested four different flow regimes according to α. In regime I ($0° < \alpha \leq 5°$), the flow separation is delayed until the trailing edge of the boat tail, and the drag is reduced accordingly (**Figure 13*a***). In regime II ($5° < \alpha \leq 15°$), a separation bubble is formed at the leading edge of the boat tail, and a strong near-wall momentum after flow reattachment delays the main separation to the trailing

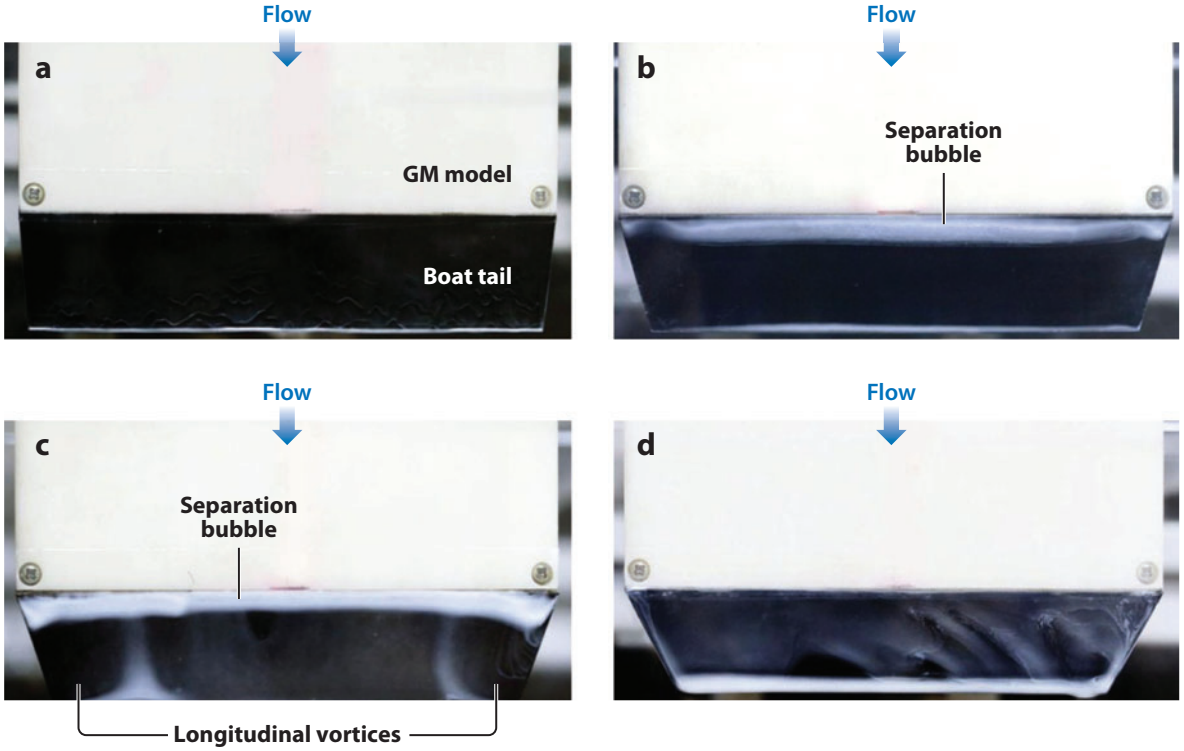

Figure 13

Oil-flow visualization on the upper plate of the boat tail attached to the GM model at $Re_H = 1.75 \times 10^5$: (*a*) $\alpha = 5°$, (*b*) 15°, (*c*) 17.5°, and (*d*) 25°. Figure taken from Yi (2007).

edge, which results in significant drag reduction (**Figure 13*b***). In regime III ($16° \leq \alpha \leq 19°$), in addition to the separation bubble, strong side longitudinal vortices are formed in the near wake and rapidly increase the drag with increasing α by generating the induced drag (**Figure 13*c***). In regime IV ($\alpha \geq 20°$), the main separation occurs at the leading edge of the boat tail, and thus the drag is the same as that experienced by the vehicle without the boat tail (**Figure 13*d***).

Croll et al. (1996) obtained drag reductions (up to 8%) on the GTS with a boat tail in a wind-tunnel experiment. However, the base cavity and boat tail are not widely adopted for real heavy vehicles because they require a significant amount of geometric modifications. Therefore, new passive or active control devices, which can be economically and legally implementable by fleet operators, still need to be developed for base drag reduction.

3.3. Underbody Drag Reduction

Underbody flow is another source of drag on a tractor-trailer; approximately 30% of the total aerodynamic drag originates from this flow (Wood 2006). Although it is one of the major sources of the drag, little effort has been invested to control the underbody flow compared to the forebody and base drag flow. So far, three devices have been suggested and tested to control the flow under a tractor-trailer (**Figure 14**): undercarriage straight skirts (Buil & Herrer 2009, Cooper & Leuschen 2005, McCallen et al. 2005, Ortega & Salari 2004, Raemdonck & Tooren 2009), belly

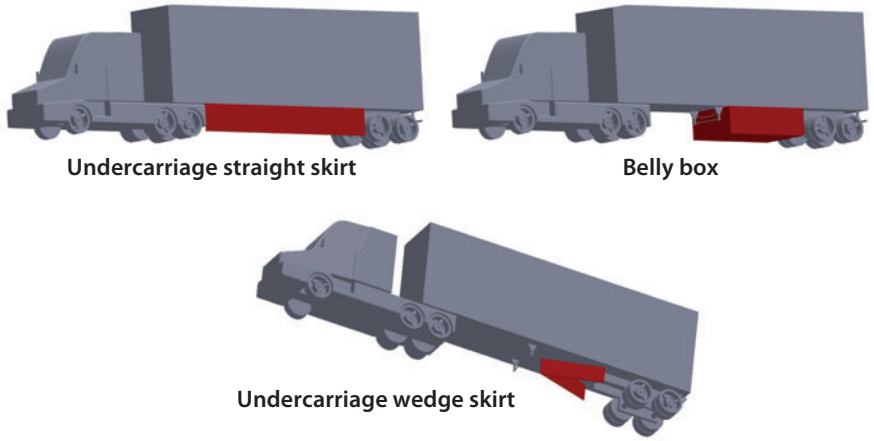

Figure 14

Devices for underbody drag reduction of a tractor-trailer: undercarriage straight skirt, belly box, and undercarriage wedge skirt. Figure reproduced from Cooper & Leuschen (2005).

boxes (Cooper & Leuschen 2005, Storms et al. 2004), and undercarriage wedge skirts (Cooper & Leuschen 2005, Ortega & Salari 2004). The purpose of the undercarriage straight skirt is to block lateral flow through the gap between the ground and the trailer body. Therefore, its drag-reduction performance improves as the yaw angle increases, but it has almost no effect at a yaw angle of zero. To compensate for this, the wedge-shaped side skirt was suggested, but it reduced the drag only near zero yaw angle (Ortega & Salari 2004). Alternatively, the belly box was shown to function as a wheelhouse enclosing the tire as well as to block the lateral flow through the ground clearance, and thus provided approximately 38% drag reduction (Storms et al. 2004).

4. FURTHER DISCUSSION

The final goals of heavy vehicle aerodynamics research are the development of effective drag-reduction devices and the control of driving stability. An accurate prediction of unsteady flow around a heavy vehicle at operating conditions is required to achieve these goals. For a tractor-trailer moving at 100 km h^{-1}, for example, the Reynolds number based on a typical trailer height is $Re_H \sim 9 \times 10^6$. Previous studies investigated the aerodynamics of a tractor-trailer at $Re_H = 1\text{–}7 \times 10^6$ through experimental (Haff et al. 2009, Storms et al. 2004) and numerical (Castellucci & Salari 2005, Tramel & Jordan 2006) approaches. These Reynolds numbers seem to be appropriate (although they are smaller than the operating Reynolds number) because the drag coefficient is known to be independent of the Reynolds number at $Re_H > 10^6$ (Hucho 1998, Storms et al. 2004). However, those studies focused mostly on the mean flow structures and statistics, but not much on localized unsteady flow phenomena. Even if unsteady flow characteristics are closely related to the mechanism of aerodynamic force generation, the current understanding of them is still insufficient. Thus, we identify a few specific unsteady flow structures around a heavy vehicle in Section 4.1 and suggest research directions for experimental and numerical approaches in Section 4.2.

4.1. Important Unsteady Flow Structures to Investigate

Heavy vehicles are frequently exposed to a crosswind during operation, by which the driving stability or the performance of a drag-reduction device varies significantly. Because the crosswind intrinsically induces unsteady, three-dimensional flow structures around the vehicles, such as unsteady flow separation and reattachment at multiple locations, massive separation, A-pillar vortices, and temporal variations of the rolling moment and side force, one should investigate them in a manner fully resolved in time and space. This requires advanced measurement techniques and high-fidelity numerical tools.

The underbody flow is another important, unresolved problem to investigate, which occurs in the gap between the vehicle body and the ground, such as the flow around a transmission system, lateral flow due to crosswind, flow around rolling tires, and flow through the engine compartment (i.e., underhood flow). The flow past rolling tires influences the cooling of the brakes and the splash/spray of water (mud), as well as the aerodynamic forces on the vehicle. The water splash/spray from rolling tires especially causes a safety problem for other vehicles or pedestrians passing by on a wet road. However, how the water sheets are formed from a rolling tire and break into multiple droplets in the wake are not fully understood and need to be examined further. The flow inside or through the engine compartment is also important for the energy efficiency of heavy vehicles, but the complex flow inside the compartment and its coupling with the temperature field have hampered our deep understanding so far. Because experimental approaches have limitations owing to complex underbody structures [e.g., reliable particle seeding and visualization for particle image velocimetry (PIV)], these flows need to be investigated mainly by numerical simulation.

Although some of the forebody and underbody drag-reduction devices are being widely adopted for heavy vehicles, there has been no real use of base drag-reduction devices. This indicates that our current understanding of the flow in the wake is still far from being sufficient to provide realistic base drag-reduction devices. Major sources for low pressure on the base of a heavy vehicle are the massive separation from the upper surface and the longitudinal vortices generated from the side edges of the slanted surface. Depending on their relative strengths and locations, the drag on the vehicle varies, as illustrated in **Figures 2** and **12**. However, estimating the aerodynamic drag resulting from each source is a very difficult task and should be studied further.

4.2. Directions for Experimental and Numerical Approaches

In heavy vehicle aerodynamics research, PIV has been used to measure local flow fields (e.g., the gap and wake flows), mostly with conventional 2D2C (two-component velocity on a two-dimensional plane) PIV. Stereo (2D3C) PIV, which measures three-component velocity fields on a two-dimensional plane, has been also applied to investigate the gap and wake flows of a tractor-trailer in a few studies (Haff et al. 2009, Heineck et al. 2004). However, only time-averaged flow fields were analyzed because the window size was not sufficiently large enough to show unsteady vortical structures in the wake at this high–Reynolds number flow. Volumetric (3D2C or 3D3C) PIV should be useful in studying the unsteady three-dimensional flow fields. For example, tomographic PIV covers a velocity range from a few micrometers per second to hundreds of meters per second in a supersonic wind-tunnel experiment (Westerweel et al. 2013), and it has a wide range of flexibility in the volume of interest, from millimeters to meters. However, volumetric PIV needs to increase its resolution in space and to be suitable for more complex geometry (Westerweel et al. 2013). With further developments of PIV techniques, one may fully resolve the unsteady, three-dimensional flow structures around a heavy vehicle.

Computational fluid dynamics has played an important role in fluid dynamics research for a wide range of problems, and it began to serve as a feasible research tool for heavy vehicle aerodynamics in the late 1980s. With fast advances in numerical methods, computing power, and parallel programming, CFD is becoming an increasingly important tool in the study of heavy vehicle aerodynamics.

In the early stages, most computational studies used the RANS equations because of their low computational cost and practicality (Han 1989, Han et al. 1996, Khalighi et al. 2001). Time-averaged flow structures such as a pair of counter-rotating vortices and a recirculation bubble in the wake, predicted by RANS simulation, showed good qualitative agreement with experimental data. However, quantitative flow variables such as the drag and mean velocity profiles showed nonnegligible deviations from the experimental data. This was attributed to the ad hoc treatments used in RANS that may not be valid for massively separated flow, i.e., a dominant flow observed in heavy vehicle aerodynamics.

LES, which solves the filtered Navier-Stokes equation with a subgrid scale (SGS) model, has been recently used to simulate unsteady flow around a vehicle (Hemida & Krajnović 2008; Howard & Pourquie 2002; Krajnović & Davidson 2003, 2005a,b; Minguez et al. 2008; Serre et al. 2013; Verzicco et al. 2002). Although various SGS models have been developed (Lesieur & Métais 1996), the most widely used one for flow over a vehicle is the eddy viscosity model based on the Smagorinsky (1963) model with a fixed model coefficient owing to its simplicity and numerical robustness. However, the Smagorinsky model with a fixed model coefficient does not accurately predict heavy vehicle aerodynamics because the model coefficient depends on the type of flow in principle but has to be provided a priori before computation. The well-known dynamic Smagorinsky model (Germano et al. 1991, Lilly 1992) overcame this weakness, but it requires a statistically homogeneous direction in the flow field for averaging the model coefficient so as to prevent numerical instability. To overcome this limitation, local averaging (Ghosal et al. 1995) and Lagrangian averaging (Meneveau et al. 1996) were suggested, but their applications to flow over a vehicle have been rare because of the free parameters used in averaging. Alternatively, the dynamic global model (Lee et al. 2010, Park et al. 2006, You & Moin 2007) does not require any flow homogeneity and determines the model coefficient based on volume averaging. This SGS model has been successfully applied to flows over various bluff bodies, including a ground vehicle (Lee & Choi 2009, Park et al. 2006), and may be a good candidate for LES of flow over a heavy vehicle.

Despite recent progress in LES, an efficient and accurate prediction of flow over a heavy vehicle using LES is still difficult to achieve, mainly because LES requires many grid points in the near-wall region at high Reynolds numbers. Chapman (1979) and Choi & Moin (2012) showed that the number of grid points required for the simulation of turbulent wall-bounded flow is significantly reduced when the near-wall dynamics is properly modeled and only a few grids are located near the wall. This approach is called a wall-modeled large-eddy simulation (WMLES), and it will be an efficient way to accurately simulate the flow around a heavy vehicle at high Reynolds numbers. Among the various WMLES approaches (Piomelli 2008, Piomelli & Balaras 2002), detached-eddy simulation (Spalart 2009, Spalart et al. 1997) has been widely adopted for vehicle aerodynamics research and is quite successful (Guilmineau et al. 2011, Hemida & Krajnović 2009, Hsu & Davis 2010, Kapadia & Roy 2003, Maddox et al. 2004). Detached-eddy simulation adopts a single turbulence model that acts as both RANS and LES closure models for the near-wall and detached regions, respectively. Another promising WMLES approach is to perform LES with the wall shear stress as the boundary condition at the wall (instead of the no-slip condition) without resolving the near-wall region (Chung & Pullin 2009, Kawai & Larsson 2012, Lee et al. 2013, Nicoud et al. 2001, Schumann 1975, Wang & Moin 2002). Typical wall-normal grid spacing at the wall

is $\Delta y^+ \gg O(10)$. The wall shear stress is dynamically obtained using the outer-layer information from outer LES or solving additional RANS equations with separate grids resolving the near-wall region. These approaches have also shown good performance in predicting canonical turbulent wall-bounded flows such as channel and boundary-layer flows. Their application to heavy vehicle aerodynamics should be an important subject in future studies.

SUMMARY POINTS

1. There are two main models for heavy vehicle aerodynamics: the Ahmed model (with varying slant angle) and GM model, which represent fast-back and square-back vehicles, respectively, both with their own time-averaged and instantaneous flow characteristics.
2. The main sources of aerodynamic forces and moments on typical heavy vehicles (e.g., tractor-trailers, buses, and HSTs) include flow separation and reattachment at various locations on the vehicle surface, a pair of longitudinal vortices from the side edges of the slanted surface, massive separation from the upper surface, and gap and underbody flow structures.
3. Drag-reduction devices for heavy vehicles can be categorized into forebody, base, and underbody drag-reduction devices, depending on the locations at which they are applied.

FUTURE ISSUES

1. Volumetric PIV techniques for high–Reynolds number flow and complex geometry should be further developed to fully understand the unsteady three-dimensional flow structures at high Reynolds numbers at which heavy vehicles are operated.
2. WMLES techniques for complex geometry should be developed and applied to flows over heavy vehicles for fast and accurate prediction.
3. New passive or active devices based on the understanding of unsteady vortical structures in the wake behind a heavy vehicle are needed for effective and practical base drag reduction.
4. More studies on the underbody flow, which is responsible for 30% of the total aerodynamic drag on a heavy vehicle, are required to predict its characteristics and to reduce the underbody aerodynamic drag.
5. The effects of crosswind on the flow structures and the rolling moment and side force on a heavy vehicle should be investigated for driving stability.

DISCLOSURE STATEMENT

The authors are not aware of any biases that might be perceived as affecting the objectivity of this review.

ACKNOWLEDGMENTS

We gratefully acknowledge financial support from the NRF programs (20120008740, R312012000100830, and 2012055647), MEST, Korea.

LITERATURE CITED

Ahmed SR, Gawthorpe RG, Mackrodt PA. 1985. Aerodynamics of road and rail vehicles. *Veh. Syst. Dyn.* 14:319–92

Ahmed SR, Ramm G, Faltin G. 1984. *Some salient features of the time-averaged ground vehicle wake*. SAE Pap. 840300, SAE Int., Warrendale, PA

Aider JL, Beaudoin JF, Wesfreid JE. 2010. Drag and lift reduction of a 3D bluff-body using active vortex generators. *Exp. Fluids* 48:771–89

Allan JW. 1981. Aerodynamic drag and pressure measurements on a simplified tractor-trailer model. *J. Wind Eng. Ind. Aerodyn.* 9:125–36

Auvity B, Bellenoue M, Kageyama T. 2001. Experimental study of the unsteady aerodynamic field outside a tunnel during a train entry. *Exp. Fluids* 30:221–28

Baker C. 2010a. The flow around high speed trains. *J. Wind Eng. Ind. Aerodyn.* 98:277–98

Baker C. 2010b. The simulation of unsteady aerodynamic cross wind forces on trains. *J. Wind Eng. Ind. Aerodyn.* 98:88–99

Balkanyi SR, Bernal LP, Khalighi B. 2002. *Analysis of the near wake of bluff bodies in ground proximity*. ASME Pap. 2002-32347, ASME, New York

Barlow JB, Guterres R, Razenbach R. 2001. Experimental parametric study of rectangular bodies with radiused edges in ground effect. *J. Wind Eng. Ind. Aerodyn.* 89:1291–309

Bearman P. 2009. Bluff body flow research with application to road vehicles. See Browand et al. 2009, pp. 3–13

Beaudoin JF, Aider JL. 2008. Drag and lift reduction of a 3D bluff body using flaps. *Exp. Fluids* 44:491–501

Bourquin V, Beguin C, Monkewitz PA. 2004. Aerodynamic effects in railway tunnels as speed is increased. See McCallen et al. 2004a, pp. 431–41

Bradley R. 2000. *Technology roadmap for the 21st century truck program*. Tech. Rep. 21CT-001, US Dep. Energy, Washington, DC

Browand F, McCallen R, Ross JC, eds. 2009. *The Aerodynamics of Heavy Vehicles II: Trucks, Buses, and Trains*. Berlin: Springer

Buil RM, Herrer LC. 2009. Aerodynamic analysis of a vehicle tanker. *J. Fluids Eng.* 131:041204

Castellucci PJ, Salari K. 2005. *Computational simulation of tractor-trailer gap flow with drag-reducing aerodynamic devices*. SAE Pap. 2005-01-3625, SAE Int., Warrendale, PA

Chapman DR. 1979. Computational aerodynamics development and outlook. *AIAA J.* 17:1293–313

Cheli F, Ripamonti F, Rocchi D, Tomasini G. 2010. Aerodynamic behaviour investigation of the new EMUV250 train to cross wind. *J. Wind Eng. Ind. Aerodyn.* 98:189–201

Choi H, Jeon WP, Kim J. 2008. Control of flow over a bluff body. *Annu. Rev. Fluid Mech.* 40:113–39

Choi H, Moin P. 2012. Grid-point requirements for large eddy simulation: Chapman's estimates revisited. *Phys. Fluids* 24:011702

Chung D, Pullin DI. 2009. Large-eddy simulation and wall modelling of turbulent channel flow. *J. Fluid Mech.* 631:281–309

Cooper KR. 1985. *The effect of front-edge rounding and rear-edge shaping on the aerodynamic drag of bluff vehicles in ground proximity*. SAE Pap. 850288, SAE Int., Warrendale, PA

Cooper KR. 2003. *Truck aerodynamics reborn: lessons from the past*. SAE Pap. 2003-01-3376, SAE Int., Warrendale, PA

Cooper KR, Leuschen J. 2005. *Model and full-scale wind tunnel tests of second-generation aerodynamic fuel saving devices for tractor-trailers*. SAE Pap. 2005-01-3512, SAE Int., Warrendale, PA

Croll RH, Gutierrez WT, Hassan B, Suazo JE, Riggins AJ. 1996. *Experimental investigation of the ground transportation systems (GTS) project for heavy vehicle drag reduction*. SAE Pap. 960907, SAE Int., Warrendale, PA

Duell EG, George AR. 1999. *Experimental study of a ground vehicle body unsteady near wake*. SAE Pap. 1999-01-0812, SAE Int., Warrendale, PA

Englar RJ. 2001. *Advanced aerodynamic devices to improve the performance, economics, handling and safety of heavy vehicles*. SAE Pap. 2001-01-2072, SAE Int., Warrendale, PA

Fago B, Lindner H, Mahrenholtz O. 1991. The effect of ground simulation on the flow around vehicles in wind tunnel testing. *J. Wind Eng. Ind. Aerodyn.* 38:47–57

Fletcher CAJ, Stewart GDH. 1986. Bus drag reduction by the trapped vortex concept for a single bus and two buses in tandem. *J. Wind Eng. Ind. Aerodyn.* 24:143–68

Germano M, Piomelli U, Moin P, Cabot WH. 1991. A dynamic subgrid-scale eddy viscosity model. *Phys. Fluids A* 3:1760–65

Geropp D, Odenthal HJ. 2000. Drag reduction of motor vehicles by active flow control using the Coanda effect. *Exp. Fluids* 28:74–85

Ghosal S, Lund TS, Moin P, Akselvoll K. 1995. A dynamic localization model for large-eddy simulation of turbulent flows. *J. Fluid Mech.* 286:229–55

Gilliéron P, Kourta A. 2010. Aerodynamic drag reduction by vertical splitter plates. *Exp. Fluids* 48:1–16

Gotz H, Mayr G. 1998. Commercial vehicles. In *Aerodynamics of Road Vehicles: From Fluid Mechanics to Vehicle Engineering*, ed. W Hucho, pp. 415–88. Warrendale, PA: SAE Int. 4th ed.

Guilmineau E, Deng G, Wackers J. 2011. Numerical simulation with a DES approach for automotive flows. *J. Fluid Struct.* 27:807–16

Gutierrez WT, Hassan B, Croll RH, Rutledge WH. 1996. *Aerodynamics overview of the ground transportation systems (GTS) project for heavy vehicle drag reduction*. SAE Pap. 960906, SAE Int., Warrendale, PA

Haff J, Jonsson M, Richard H, Loose S. 2009. Experimental investigation on a detailed European tractor-trailer configuration. See Paschereit 2009, pp. 104–15

Hammache M, Browand F. 2004. On the aerodynamics of tractor-trailers. See McCallen et al. 2004a, pp. 185–205

Han T. 1989. Computational analysis of three-dimensional turbulent flow around a bluff body in ground proximity. *AIAA J.* 27:1213–19

Han T, Hammond DC Jr, Sagi CJ. 1992. Optimization of bluff body for minimum drag in ground proximity. *AIAA J.* 30:882–89

Han T, Sumantran V, Harris C, Kuzmanov T, Huebler M, Zak T. 1996. *Flow-field simulations of three simplified vehicle shapes and comparisons with experimental measurements*. SAE Pap. 960678, SAE Int., Warrendale, PA

Heineck JT, Walker SM, Satran D. 2004. The measurement of wake and gap flows of the generic conventional truck model (GCM) using three-component PIV. See McCallen et al. 2004a, pp. 173–84

Hemida H, Krajnović S. 2008. LES study of the influence of a train-nose shape on the flow structures under cross-wind conditions. *J. Fluids Eng.* 130:091101

Hemida H, Krajnović S. 2009. Transient simulation of the aerodynamic response of a double-deck bus in gusty winds. *J. Fluid Eng.* 131:031101

Herbst AH, Mauss J, Heiland J, Orellano A. 2009. Shape optimization in train aerodynamics. See Paschereit 2009, pp. 116–27

Hinterberger C, García-Villalba M, Rodi W. 2004. Large eddy simulation of flow around the Ahmed body. See McCallen et al. 2004a, pp. 77–89

Howard RJA, Pourquie M. 2002. Large eddy simulation of an Ahmed reference model. *J. Turbul.* 3:1–18

Howell J, Sheppard A, Blakemore A. 2003. *Aerodynamic drag reduction for a simple bluff body using base bleed*. SAE Pap. 2003-01-0995, SAE Int., Warrendale, PA

Hsu F, Davis RL. 2010. Drag reduction of tractor-trailers using optimized add-on. *J. Fluid Eng.* 132:084504

Hucho WH. 1998. *Aerodynamics of Road Vehicles.* Warrendale, PA: SAE Int.

Hucho WH, Janssen LJ, Emmelmann HJ. 1976. *Optimization of body details: a method for reducing the aerodynamic drag of road vehicles*. SAE Pap. 760185, SAE Int., Warrendale, PA

Hucho WH, Sovran G. 1993. Aerodynamics of road vehicles. *Annu. Rev. Fluid Mech.* 25:485–537

Hunt JCR, Wray AA, Moin P. 1988. *Eddies, stream, and convergence zones in turbulent flows*. CTR-S88, Cent. Turbul. Res., Stanford Univ., Stanford, CA

Hwang J, Yoon TS, Lee DH, Lee SG. 2001. Numerical study of unsteady flowfield around high speed trains passing by each other. *JSME Int.* 44:451–64

Hyams DG, Sreenivas K, Pankajakshan R, Nichols DS, Briley WR, Whitfield DL. 2011. Computational simulation of model and full scale Class 8 trucks with drag reduction devices. *Comput. Fluids* 41:27–40

Kapadia S, Roy S. 2003. *Detached-eddy simulation over a reference Ahmed car model*. Presented at Aerosp. Sci. Meet. Exhib., 41st, Reno, NV, AIAA Pap. 2003-0857

Kawai S, Larsson J. 2012. Wall-modeling in large eddy simulation: length scales, grid resolution, and accuracy. *Phys. Fluids* 24:015105

Khalighi B, Zhang S, Koromilas C, Balkanyi SR, Bernal LP, et al. 2001. *Experimental and computational study of unsteady wake flow behind a bluff body with a drag reduction device*. SAE Pap. 2001-01B-207, SAE Int., Warrendale, PA

Khier W, Breuer M, Durst F. 2000. Flow structure around trains under side wind conditions: a numerical study. *Comput. Fluids* 29:179–95

Krajnović S. 2009. Shape optimization of high-speed trains for improved aerodynamic performance. *Proc. Inst. Mech. Eng. Part F J. Rail Rapid Transit* 223:439–52

Krajnović S, Davidson L. 2003. Numerical study of the flow around a bus-shaped body. *J. Fluids Eng.* 125:500–9

Krajnović S, Davidson L. 2005a. Flow around a simplified car, part 1: large eddy simulation. *J. Fluids Eng.* 127:907–18

Krajnović S, Davidson L. 2005b. Flow around a simplified car, part 2: understanding the flow. *J. Fluids Eng.* 127:919–28

Krajnović S, Davidson L. 2005c. Influence of floor motions in wind tunnels on the aerodynamics of road vehicles. *J. Wind Eng. Ind. Aerodyn.* 93:677–96

Krajnović S, Hafsteinsson HE, Helgason E, Basara B. 2009. Shape optimization of a bus for crosswind stability. See Paschereit 2009, pp. 162–73

Lee J, Cho M, Choi H. 2013. Large eddy simulations of turbulent channel and boundary layer flows at high Reynolds number with mean wall shear stress boundary condition. *Phys. Fluids* 25:110808

Lee J, Choi H. 2009. Large eddy simulation of flow over a three-dimensional model vehicle. *Proc. 6th Int. Symp. Turbul. Shear Flow Phenom.*, Vol. 1, ed. N Kasagi, JK Eaton, R Friedrich, JAC Humphrey, AV Johansson, HJ Sung, pp. 735–39

Lee J, Choi H, Park N. 2010. Dynamic global model for large eddy simulation of transient flow. *Phys. Fluids* 22:075106

Le Good GM, Garry KP. 2004. *On the use of reference models in automotive aerodynamics*. SAE Pap. 2004-01-1308, SAE Int., Warrendale, PA

Lesieur M, Métais O. 1996. New trends in large-eddy simulations of turbulence. *Annu. Rev. Fluid Mech.* 28:45–82

Leuschen J, Cooper KR. 2009. Summary of full-scale wind tunnel tests of aerodynamic drag-reducing devices for tractor-trailers. See Browand et al. 2009, pp. 451–62

Lilly D. 1992. A proposed modification of the Germano subgrid-scale closure method. *Phys. Fluids A* 4:633–35

Littlewood RP, Passmore MA. 2012. Aerodynamic drag reduction of a simplified squareback vehicle using steady blowing. *Exp. Fluids* 53:519–29

Maddox S, Squires KD, Wurtzler KE, Forsythe JR. 2004. Detached-eddy simulation of the ground transportation system. See McCallen et al. 2004a, pp. 89–104

Malviya V, Mishra R, Fieldhouse J. 2009. CFD investigation of a novel fuel-saving device for articulated tractor-trailer combinations. *Eng. Appl. Comput. Fluid Mech.* 3:587–607

McCallen R, Browand F, Ross JC, eds. 2004a. *The Aerodynamics of Heavy Vehicles: Trucks, Buses, and Trains*. Berlin: Springer

McCallen RC, Salari K, Ortega J, Castellucci P, Eastwood C, et al. 2005. *DOE project on heavy vehicle aerodynamic drag FY 2005 annual report*. Rep. UCRL-TR-217193, Lawrence Livermore Natl. Lab., Livermore, CA

McCallen RC, Salari K, Ortega J, DeChant LJ, Hassan B, et al. 2004b. *DOEs effort to reduce truck aerodynamic drag: Joint experiments and computations lead to smart design*. Presented at AIAA Fluid Dyn. Conf. Exhib., 34th, Portland, OR, AIAA Pap. 2004-2249

McManus J, Zhang X. 2006. A computational study of the flow around an isolated wheel in contact with the ground. *J. Fluids Eng.* 128:520–30

Meneveau C, Lund TS, Cabot WH. 1996. A Lagrangian dynamic subgrid-scale model of turbulence. *J. Fluid Mech.* 319:353–85

Mercker E, Bernerburg H. 1992. *On the simulation of road driving of a passenger car in a wind tunnel using a moving belt and rotating wheels*. Presented at Int. Conf. Innov. Reliab., 3rd, Florence, Fr.

Minguez M, Pasquetti R, Serre E. 2008. High-order large-eddy simulation of flow over the "Ahmed body" car model. *Phys. Fluids* 20:095101

Mohamed-Kassim Z, Filippone A. 2010. Fuel savings on a heavy vehicle via aerodynamic drag reduction. *Transport. Res. D* 15:275–84

Mok JK, Yoo J. 2001. Numerical study on high speed train and tunnel hood interaction. *J. Wind Eng. Ind. Aerodyn.* 89:17–29

Muirhead VU, Saltzman EJ. 1979. Reduction of aerodynamic drag and fuel consumption for tractor-trailer vehicles. *J. Energy* 3:279–84

Nicoud F, Baggett JS, Moin P, Cabot W. 2001. Large eddy simulation wall-modeling based on suboptimal control theory and linear stochastic estimation. *Phys. Fluids* 13:2968–84

Ortega JM, Dunn T, McCallen R, Salari K. 2004. Computational simulation of a heavy vehicle trailer wake. See McCallen et al. 2004a, pp. 219–33

Ortega JM, Salari K. 2004. *An experimental study of drag reduction devices for a trailer underbody and base*. Presented at AIAA Fluid Dyn. Conf. Exhib., 34th, Portland, OR, AIAA Pap. 2004-2252

Ortega JM, Salari K, Storms B. 2007. *Investigation of tractor base bleeding for heavy vehicle aerodynamic drag reduction*. Rep. UCRL-PROC-235892, Lawrence Livermore Natl. Lab., Livermore, CA

Östh J, Krajnović S. 2012. The flow around a simplified tractor-trailer model studied by large eddy simulation. *J. Wind Eng. Ind. Aerodyn.* 102:36–47

Pankajakshan R, Mitchell B, Whitfield DL. 2009. Full-scale simulations of drag reduction device for Class 8 trucks. See Browand et al. 2009, pp. 339–48

Park N, Lee S, Lee J, Choi H. 2006. A dynamic subgrid-scale eddy viscosity model with a global model coefficient. *Phys. Fluids* 18:125109

Paschereit CO, ed. 2009. *Proceedings of Euromech Colloquium 509: External Aerodynamics of Railway Vehicles, Trucks, Buses and Cars*. Berlin: Eur. Mech. Soc.

Paschkewitz JS. 2006. *Simulation of spray dispersion in a simplified heavy vehicle wake*. Rep. UCRL-TR-218207. Lawrence Livermore Natl. Lab., Livermore, CA

Peterson RL. 1981. *Drag reduction obtained by the addition of a boattail to a box shaped vehicle*. Rep. NASA-CR-163113. NASA, Washington, DC

Piomelli U. 2008. Wall-layer models for large-eddy simulations. *Prog. Aerosp. Sci.* 44:437–46

Piomelli U, Balaras E. 2002. Wall-layer models for large-eddy simulations. *Annu. Rev. Fluid Mech.* 34:349–74

Pirozzoli S, Orlandi P, Bernardini M. 2012. The fluid dynamics of rolling wheels at low Reynolds number. *J. Fluid Mech.* 706:496–533

Pujals G, Depardon S, Cossu C. 2010. Drag reduction of a 3D bluff body using coherent streamwise streaks. *Exp. Fluids* 49:1085–94

Raemdonck GV, Tooren MV. 2009. A practical scientific approach for aerodynamic truck design. See Paschereit 2009, pp. 293–303

Raghunathan RS, Kim HD, Setoguchi T. 2002. Aerodynamics of high-speed railway train. *Prog. Aerosp. Sci.* 38:469–514

Regert T, Lajos T. 2007. Description of flow field in the wheelhouse of cars. *Int. J. Heat Fluid Flow* 28:616–29

Ricco P, Baron A, Molteni P. 2007. Nature of pressure waves induced by a high-speed train travelling through a tunnel. *J. Wind Eng. Ind. Aerodyn.* 95:781–808

Roy CJ, Payne J, McWherter-Payne M. 2006. RANS simulations of a simplified tractor/trailer geometry. *J. Fluid Eng.* 128:1083–89

Salari K. 2006. *Heavy vehicle drag reduction devices: computational evaluation and design*. Presented at 2006 US Dep. Energy Heavy Veh. Syst. Rev., Argonne, IL, Apr. 18–20

Salari K, Ortega JM, Castellucci PJ. 2004. *Computational prediction of aerodynamic forces for a simplified integrated tractor-trailer geometry*. Presented at AIAA Fluid Dyn. Conf. Exhib., 34th, Portland, OR., AIAA Pap. 2004-2253

Schetz JA. 2001. Aerodynamics of high-speed trains. *Annu. Rev. Fluid Mech.* 33:371–414

Schumann U. 1975. Subgrid scale model for finite difference simulations of turbulent flows in plane channels and annuli. *J. Comput. Phys.* 18:376–404

Serre E, Minguez M, Pasquetti R, Guilmineau E, Deng GB, et al. 2013. On simulating the turbulent flow around the Ahmed body: a French-German collaborative evaluation of LES and DES. *Comput. Fluids* 78:10–23

Siewny M, Bellman M, Agarwal R. 2010. *Numerical drag reduction studies of generic truck models in ground effect using active flow control*. Presented at AIAA Fluid Dyn. Conf. Exhib., 40th, Chicago, AIAA Pap. 2010-4593

Smagorinsky J. 1963. General circulation experiments with primitive equations I. The basic experiments. *Mon. Weather Rev.* 91:99–164

Spalart PR. 2009. Detached-eddy simulation. *Annu. Rev. Fluid Mech.* 41:181–202

Spalart PR, Jou WH, Strelets M, Allmaras SR. 1997. Comments on the feasibility of LES for wings and on a hybrid RANS/LES approach. In *Advances in DNS/LES*, ed. C Liu, Z Liu, pp. 137–47. Columbus, OH: Greyden

Sreenivas K, Pankajakshan R, Nichols DS, Mitchell BCJ, Taylor LK, Whitfield DL. 2006. *Aerodynamic simulation of heavy trucks with rotating wheels*. Presented at AIAA Aerosp. Sci. Meet. Exhib., 44th, Reno, NV, AIAA Pap. 2006-1394

Steers LL, Saltzman EJ. 1977. Reduced truck fuel consumption through aerodynamic design. *J. Energy* 1:312–18

Storms BL, Ross JC, Heineck JT, Walker SM, Driver DM, Zilliac GG. 2001. *An experimental study of the ground transportation system (GTS) model in the NASA Ames 7- by 10-ft wind tunnel*. NASA Tech. Rep. 2001-209621, NASA Ames Res. Cent., Moffett Field, CA

Storms BL, Satran DR, Heineck JT, Walker SM. 2004. *A study of Reynolds number effects and drag-reduction concepts on a generic tractor-trailer*. Presented at AIAA Fluid Dyn. Conf. Exhib., 34th Portland, OR, AIAA Pap. 2004-2251

Strachan RK, Knowles K, Lawson NJ. 2007. The vortex structure behind an Ahmed reference model in the presence of a moving ground plane. *Exp. Fluids* 42:659–69

Thacker A, Aubrun S, Leroy A, Devinant P. 2010. *Unsteady analyses of the flow separation on the rear window of a simplified ground vehicle model*. Presented at AIAA Appl. Aerodyn. Conf., 28th, Chicago, AIAA Pap. 2010-4569

Thacker A, Aubrun S, Leroy A, Devinant P. 2012. Effects of suppressing the 3D separation on the rear slant on the flow structures around an Ahmed body. *J. Wind Eng. Ind. Aerodyn.* 107–108:237–43

Tramel RW, Jordan JK. 2006. *Evaluation of RANS turbulence models for a generic tractor-trailer configuration*. Presented at AIAA Appl. Aerodyn. Conf., 24th, San Francisco, AIAA Pap. 2006-3859

Verzicco R, Fatica M, Iaccarino G, Moin P, Khalighi B. 2002. Large eddy simulation of a road vehicle with drag-reduction devices. *AIAA J.* 40:2447–55

Vino G, Watkins S, Mousley P, Watmuff J, Prasad S. 2005. Flow structures in the near-wake of the Ahmed model. *J. Fluids Struct.* 20:673–95

Wang M, Moin P. 2002. Dynamic wall modeling for large-eddy simulation of complex turbulent flows. *Phys. Fluids* 14:2043–51

Westerweel J, Elsinga GE, Adrian RJ. 2013. Particle image velocimetry for complex and turbulent flows. *Annu. Rev. Fluid Mech.* 45:409–36

Wickern G, Zwicker K, Pfadenhauer M. 1997. *Rotating wheels: their impact on wind tunnel test techniques and on vehicle drag results*. SAE Pap. 970133, SAE Int., Warrendale, PA

Wong DTM, Mair WA. 1983. Boat-tailed afterbodies of square section as drag-reduction devices. *J. Wind Eng. Ind. Aerodyn.* 12:229–35

Wood RM. 2006. *A discussion of a heavy truck advanced aerodynamic trailer system*. Presented at Int. Symp. Heavy Veh. Weights Dimens., 9th, University Park, PA

Wood RM, Bauer SXS. 2003. *Simple and low-cost aerodynamic drag reduction devices for tractor-trailer trucks*. SAE Pap. 2003-01-3377, SAE Int., Warrendale, PA

Yi W. 2007. *Drag reduction of a three-dimensional car model using passive control device.* PhD diss. Seoul Natl. Univ.

You D, Moin P. 2007. A dynamic global-coefficient subgrid-scale eddy-viscosity model for large-eddy simulation in complex geometries. *Phys. Fluids* 19:065110

Zhang X, Toet W, Zerihan J. 2006. Ground effect aerodynamics of race cars. *Appl. Mech. Rev.* 59:33–49

Annual Review of
Fluid Mechanics

Volume 46, 2014

Contents

Indexes

Errata

An online log of corrections to *Annual Review of Fluid Mechanics* articles may be found at http://fluid.annualreviews.org/errata.shtml